MAGNETIC MOMENT AND MAGNETIZATION

Michael E. McHenry and David E. Laughlin
Carnegie Mellon University, Pittsburgh, PA, USA

INTRODUCTION

Magnetism has engaged explorers and scientists for over two millennia. The ancient Greeks and Turks noted the attraction between *magnetite* (*lodestone*) and iron (Cullity and Graham, 1978). Explorers used lodestone's *magnetization* to construct compass needles used to point to the direction of the earth's magnetic North Pole. This singularly important device aided in navigation and the exploration of the planet. Today, the miniaturization of magnetic sensors has propelled the magnetic recording industry as well as contributed to far-reaching applications such as planetary exploration (Diaz-Michelena, 2009).

Michael Faraday's (1791–1867) discovery of *electromagnetic induction* provides the principle for understanding the operation of electric generators, transformers, and a variety of other magnetic devices. The quantum mechanical description of the origin of *atomic magnetic dipole moments* provides the basis for understanding a variety of disparate phenomena including the magnetic response of materials.

The intrinsic magnetic properties of materials refer to:

i. the origin, magnitude, and directions of atomic magnetic dipole moments;
ii. the nature of the interaction between atomic magnetic dipole moments on neighboring atoms in the solid;
iii. whether these result in collective magnetic phenomena; and
iv. the resulting temperature dependence of the magnetization.

For materials exhibiting *collective magnetic response*, other intrinsic magnetic properties include the strength of the coupling of magnetic moments to one another and to crystallographic directions, magnetoelastic coupling coefficients, and the temperature(s) at which magnetic phase transformations occur. The intrinsic magnetic properties, of species at surfaces and interfaces, are known to be distinctly different from those of the bulk in many cases. This article reviews the theory of intrinsic magnetic properties of dipole moment and magnetization as well as theory and examples of collective magnetic response. The National Institute of Standards and Technology (NIST) keeps an up-to-date compilation of units. These can be found in R. B. Goldfarb and F. R. Fickett, U.S. Department of Commerce, National Bureau of Standards, Boulder, Colorado 80303, March 1985 NBS Special Publication 696 for sale by the Superintendent of Documents, U.S. Government Printing Office, Washington, DC 20402.

DEFINITIONS OF FIELD QUANTITIES

Discussion of the magnetic properties of materials begins by defining macroscopic field quantities.[1] The two fundamental quantities are the *magnetic induction*, $\vec{B}$, and the *magnetic field*, $\vec{H}$, both of which are axial vector quantities. In many cases the induction and the field will be collinear (parallel) so that we can treat them as scalar quantities, B and H.[2]

In a vacuum, the magnetic induction, $\vec{B}$, is related to the magnetic field, $\vec{H}$:

$$\vec{B} = \mu_0 \vec{H}, \qquad \vec{B} = \vec{H} \tag{1}$$

where the *permeability of the vacuum*, μ_0, is $4\pi \times 10^{-7}$ H/m in SI (mksa) units. This quantity is taken as 1 in cgs units. In cgs units, the induction and field have the same values. In SI (mksa) units we assign a permeability to the vacuum, so the two are proportional.

In a magnetic material the magnetic induction can be enhanced or reduced by the material's *magnetization*, $\vec{M}$ (defined as net dipole moment per unit volume), so that

$$\vec{B} = \mu_0(\vec{H} + \vec{M}), \qquad \vec{B} = \vec{H} + 4\pi\vec{M} \tag{2}$$

where the magnetization, $\vec{M}$, is expressed in linear response theory as

$$\vec{M} = \chi_m \vec{H} \tag{3}$$

and the constant of proportionality is called the *magnetic susceptibility*, χ_m. The magnetic susceptibility that relates two vector quantities is a polar second-rank tensor. For most discussions (whenever B and H are collinear or when interested in the magnetization component in the field direction) we treat the susceptibility as a scalar.

We continue our discussion considering scalar induction, field, and magnetization. We can further express $B = \mu_r H$ as

$$B = \mu_0(1 + \chi_m)H, \qquad B = (1 + 4\pi\chi_m)H \tag{4}$$

and we see that the *relative permeability*, μ_r, can be expressed as

$$\mu_r = \mu_0(1 + \chi_m), \qquad \mu_r = 1 + 4\pi\chi_m \tag{5}$$

μ_r thus represents an enhancement factor of the flux density in a magnetic material due to the magnetization that is an intrinsic material property. If we have $\chi_m < 0$, we speak of diamagnetic response, and for $\chi_m > 0$ (and no *collective magnetism*) we speak of *paramagnetic*

[1] Selected formulas are introduced in SI (mksa) units followed by cgs units.
[2] For many discussions it is sufficient to treat field quantities as scalars; when this is not the case, vector symbols will be explicitly used.

Characterization of Materials, edited by Elton N. Kaufmann.

response. A *superconductor* is a material that acts as a *perfect diamagnet* so that $\chi_m = -1$ or $\chi_m = \dfrac{-1}{4\pi}$.

MAGNETIC DIPOLE MOMENTS—DEFINITIONS AND ATOMIC ORIGINS

A *magnetic dipole moment* has its origin in circulating charge (Fig. 1). This concept is made more complicated by the need to treat circulating charges of electrons within the framework of quantum mechanics.

Concepts relating circulating charge, angular momentum, and dipole moments are:

i. A dipole moment for a circulating charge is defined formally as

$$\vec{\mu} = IA\vec{u}_{\vec{r}\times\vec{J}} = \int_V \vec{r}\times\vec{J}\, dV \tag{6}$$

where $\vec{r}$ is the position vector of the charged particle about the origin for the rotation. $\vec{r}$ is the current density of the orbiting charge. I is the current due to the circulating charge, $A = \pi r^2$ is the area swept out by the circulating charge, and V is the volume. $\vec{u}_{\vec{r}\times\vec{J}}$ is a unit vector normal to the area, A.

ii. We relate the magnetic dipole moment to the *angular momentum*. Let $\vec{\Pi}$ be a general angular momentum vector. In classical mechanics, the angular momentum vector, expressed as $\vec{\Pi} = \vec{r}\times m\vec{v}$, has magnitude $mvr = m\omega_0 r^2$, where ω_0 is an angular frequency, and is directed normal to the current loop (parallel to the dipole moment). The fundamental relationship between magnetic dipole moment and the angular momentum vector is

$$\mu = g\frac{e}{2m}\Pi, \qquad \mu = g\frac{e}{2mc}\Pi \tag{7}$$

where g is called the *Lande g-factor*. For an orbiting electron the constant $g = 1$. The dipole moment associated with *spin angular momentum* has $g = 2$.

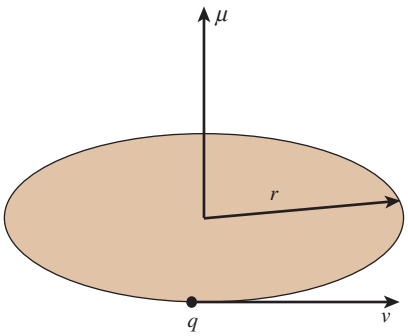

Figure 1. Geometry of a charged particle orbiting at a distance r, with a linear velocity, v. The particle orbit sweeps out an area, A, and gives rise to a dipole moment, $\vec{\mu}$.

iii. In quantum mechanics, every electron has a dipole moment associated with its spinning charge density (spin) and its orbit about the nucleus (orbit). Angular momentum (whether spin or orbital) is quantized in units of **Planck's constant** divided by 2π, that is, $\hbar = \dfrac{h}{2\pi} = 1.05\times 10^{-34}$ J s $= 1.05\times 10^{-27}$ erg s. We define the fundamental unit of magnetic dipole moment, the *Bohr magneton*, as

$$\mu_B = \frac{e}{2m}\hbar, \qquad \mu = \mu_B = \frac{e}{2mc}\hbar \tag{8}$$

The Bohr magneton is calculated to have the following value:

$$\mu_B = 9.27\times 10^{-24}\ \text{Am}^2\ (\text{J/T}),$$
$$\mu = \mu_B = 9.27\times 10^{-21}\ \text{erg/G} \tag{9}$$

iv. An atomic dipole moment is calculated by summing all of the electron dipole moments for a given atomic species. Quantum mechanical rules for this summing called *Hund's rules* are discussed below.

v. For a collection of identical atoms the magnetization, M, is

$$M = N_a\mu_{atom} \tag{10}$$

where N_a is the number of dipole moments per unit volume and μ_{atom} is the atomic dipole moment.

vi. The potential energy of a dipole moment in the presence of a field is

$$E_p = \vec{\mu}\cdot\vec{B} = \mu B\cos\theta \tag{11}$$

where θ is the angle between the dipole moment and $\vec{B}$. This implies that magnetization (or other field quantity) multiplied by another field has units of energy per unit volume. It is important to begin to think of energy densities (energy per unit volume) for magnetic systems. In quantum mechanical systems, the component of the dipole moment vector projected along the field direction is quantized and only particular values of the angle θ are allowed.

Closed Shell Diamagnetism: Langevin Theory of Diamagnetism

The diamagnetic susceptibility of closed shells is discussed in Box 1.

> Diamagnetism is the atomic magnetic response due to closed shell orbits of core electrons.

This is to be contrasted with the perfect diamagnetism of a *superconductor*. Magnetic flux is excluded from the interior of a superconductor and it is a consequence of $B = 0$, which requires that $\chi_m = -1$ or $\chi_m = \dfrac{-1}{4\pi}$.

MAGNETIC SUSCEPTIBILITY OF A SIMPLE DIAMAGNET

Consider an atom with a closed electronic shell. For filled shells, electrons orbit the nuclei, but the net current associated with their motion is zero because of cancellation of their summed orbital angular momentum, $\vec{L}$ (i.e., $\vec{L} = 0$). However, even for a closed shell, in the presence of an applied field a net current is induced. By *Lenz's law* this current results in a dipole moment that opposes the applied field. The *Larmor frequency*, ω_L, is the characteristic frequency of this circulating induced current and has a value

$$\omega_L = \frac{eH}{m}, \qquad \omega_L = \frac{eH}{mc} \tag{12a}$$

If we wish to construct an atomic dipole moment, we must consider the moment due to Z electrons that orbit the nucleus. Assuming that all Z electrons orbit the nucleus with the same angular frequency, ω_L, we express the current, I, as follows:

$$I = \frac{dq}{dt} = \frac{Ze\omega_L}{2\pi} \tag{12b}$$

The induced moment is calculated as the current multiplied by the area and the orbital atomic magnetic dipole moment is then

$$\mu_{atom} = -\frac{Ze\omega_L}{2}\frac{\langle r^2\rangle}{3} \tag{12c}$$

where the minus sign reflects Lenz's law and $\langle r^2\rangle$ is the average value of r^2 for the orbit. The average value of the square of the orbital radius is

$$\langle r^2\rangle = \langle x^2\rangle + \langle y^2\rangle + \langle z^2\rangle \tag{12d}$$

and for an isotropic environment:

$$\langle x^2\rangle = \langle y^2\rangle = \langle z^2\rangle = \frac{\langle r^2\rangle}{3} \tag{12e}$$

This may be associated with the negative diamagnetic susceptibility (for N atoms/volume):

$$\chi_m = \frac{N\mu_{atom}}{H} = -\frac{NZe^2}{6m}, \qquad \chi_m = \frac{N\mu_{atom}}{H} = -\frac{NZe^2}{6mc} \tag{12f}$$

which describes well the diamagnetism of core electrons and of closed shell systems. Typically molar diamagnetic susceptibilities are on the order of $\chi_m = 10^{-6}$ to 10^{-5} cm^3/mol $= 10^{-12}$ to 10^{-11} m^3/mol.

The magnitude, $L = |\vec{L}|$, of the orbital angular momentum vector, $\vec{L}$, and its projection, L_z, onto an axis of quantization, z, by the application of a field, B_z, is quantized in units of $\hbar$. For L_z the quantum number m_l quantizes the projected orbital angular momentum. This has the further consequence that the orbital angular momentum vector, $\vec{L}$, can precess about the field axis, z, only at a set of discrete angles, θ:

$$L_z = m_l\hbar, \qquad m_l = -l \cdots 0 \cdots +l,$$
$$\theta = \arccos\frac{L_z}{L} = \arccos\frac{m_l}{l} \tag{13}$$

Open Shell Atomic Dipole Moments—Hund's Rules

We now examine systems where the electrons responsible for the dipoles exist in *localized states* assigned to a particular atom. In systems (typically ionic) where the atomic orbitals responsible for the magnetic dipole moments are localized on specific atoms in a solid, discrete magnetic states can be calculated using quantum mechanical rules called *Hund's rules* (Hund, 1927). This discussion is applicable in understanding the magnetic dipoles in ionic systems such as oxides and salts of transition metals.

A general angular momentum vector, $\vec{\Pi}$, can have contributions from *orbital angular momentum*, $\vec{L}$, and *spin angular momentum*, $\vec{S}$. Both moments are quantized in units of $\hbar$. The fundamental atomic unit of dipole moment is the Bohr magneton.

In addition to the orbital moment, there is an additional contribution to the magnetic moment of an electron, due to spin. Spin is a purely quantum mechanical property though we can view it semiclassically considering an electron as a particle with a rotating surface current. The classical problem yields a spin moment similar to that which is derived in the quantum mechanical description (Cullity and Graham, 1978).

Determining atomic dipole moments requires summing spin and orbital angular momenta over all electrons on an atom. The summed orbital and spin angular momenta is zero for closed shells. The closed shells then only contribute to the small diamagnetic moment of the previous section.[3] In open shells we need to consider rules for summing the spin and orbital angular momenta for all electrons in the open shell. Hund's rules allow us to describe the ground-state multiplet including the m_l and m_s eigenstates and allow us to calculate the components of the orbital, L, spin, S, and total angular, J, momenta. The magnitudes of orbital and spin angular momenta are constructed by summing angular momentum over a multielectron shell:

$$L = \sum_{i=1}^{n}(m_l)_i\hbar, \qquad S = \sum_{i=1}^{n}2(m_s)_i\hbar \tag{14}$$

The projection of the total angular momentum vector, $\vec{J} = \vec{L} + \vec{S}$, along the applied field direction is also subject to quantization conditions. Hund's rules require that J ($J = L + S$) is $|L-S|$ for less than half-filled shells and $|L+S|$ for greater than half-filled shells. To determine the occupation of eigenstates of S, L, and

[3] For open shells this diamagnetic contribution is small enough to ignore.

J we use Hund's rules that state that for a closed electronic shell $J = L = S = 0$. For an open shell multi-electron atom:

i. We fill m_l states (which are $(2l+1)$-fold degenerate) in such a way as to first maximize total spin.
ii. We fill m_l states first in such a way as to first maximize total spin.

We consider the ions of transition metal series, TM^{2+}, that is, ions that have given up 2s electrons to yield a $3d^n$ outer shell configuration in Figure 2a. The ground-state J, L, and S quantum numbers for rare earth, RE^{3+}, ions are shown in Figure 2b.

Defining L, S, and J for a given element specifies the ground-state multiplet. This multiplet is written more compactly in the spectroscopic term symbol as

$$^{2S+1}L_J \tag{15}$$

where L is the alphabetic symbol for orbital angular momentum ($L = 0 = S$, $L = 1 = P$, $L = 2 = D$, $L = 3 = F$, etc.) and $2S+1$ and J are the numerical values of the same. For example, Cr^{3+} with $L = 3$, $S = \frac{3}{2}$, and $J = \frac{3}{2}$ would be assigned the term symbol $^4L_{3/2}$. We can further relate the permanent local atomic moment vector with the total angular momentum vector, $\vec{J}$, as

$$\vec{\mu} = \gamma\hbar\vec{J} = -g(J,L,S)\mu_B\vec{J} \tag{16a}$$

where γ is called the *gyromagnetic factor* and $g = g(J,L,S)$ is called the *Lande g-factor* and is given by

$$g(J,L,S) = \frac{3}{2} + \frac{1}{2}\left[\frac{S(S+1)-L(L+1)}{J(J+1)}\right] \tag{16b}$$

Table 1 tabulates the ground-state multiplets for transition metal and rare earth cation species that are prevalent in many oxides and other interesting ionic systems.

The Lande g-factor accounts for precession of angular momentum and quantum mechanical rules for projection onto the field axis (Fig. 3) (Russell and Saunders, 1925). For identical ions with angular momentum J we define an effective magnetic moment in units of μ_B:

$$p_{\text{eff}} = g(J,L,S)[J(J+1)]^{1/2} \tag{17}$$

As an example of the calculation of a Hund's rule ground state, we consider the Ho^{3+} multiplet. Ho^{3+} has a $4f^{10}$ open shell configuration. According to Hund's rules we occupy the 7 m_l states with spin-up electrons followed by $m_l = -3, -2, -1$ to account for all 10 outer shell f electrons (note that the 2 outer shell s and 1 outer shell d electron of the atom are those that are lost in ionization). For Ho^{3+}, we see that $S = \frac{7}{2} - \frac{3}{2} = 2$ and $L = |-3-2-1| = 6$ and since the f shell is more than half-filled, $J = L + S = 8$. The term symbol for Ho^{3+} is therefore $^5I_8$. The Lande g-factor can be calculated to be

$$g(J,L,S) = \frac{3}{2} + \frac{1}{2}\left[\frac{2(2+1)-6(6+1)}{8(8+1)}\right]$$
$$= \frac{3}{2} + \frac{1}{2}\left[\frac{6-42}{72}\right] = 1.25$$

and the effective moment in units of μ_B is

$$p_{\text{eff}} = g(J,L,S)[J(J+1)]^{1/2}\mu_B = 1.25[72]^{1/2}\mu_B = 7.5\sqrt{2}\,\mu_B$$

Dipole Moments in Systems with Quenched Orbital Angular Momentum

In many systems of interest the orbital angular momentum is said to be quenched. The *quenched orbital angular momentum* refers to the fact that the orbital angular moment vector is strongly tied to a crystalline *easy magnetization direction* (*EMD*). For this reason to a good approximation we can take $L = 0$ and $J = S$. In this case $g = 2$ and $p_{\text{eff}} = 2[S(S+1)]^{1/2}$. This is true for many transition metal systems and also for simple oxides of the transition metals. The relationship between magnetic dipole moment, μ, and angular momentum vector is given by $\mu = g\frac{e}{2m}\Pi$, where Π can refer to orbital, $\vec{L}$, or spin, $\vec{S}$, angular momentum and g is the gyromagnetic factor. In ferrites the d shells of transition metal cations are of interest, and we have *quenched orbital angular momentum* (i.e., $\vec{L} = 0$) in the crystal. The spin angular momentum for a single electron is quantized by the spin quantum number, $m_s = \pm\frac{1}{2}$, to be $m_s\hbar = \pm\frac{\hbar}{2}$. For spin

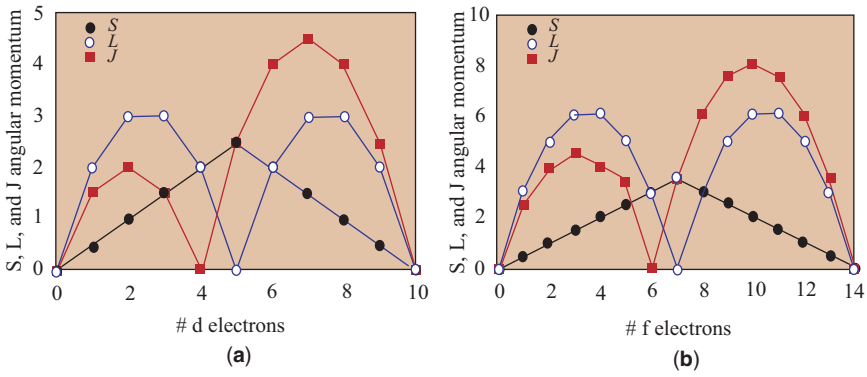

Figure 2. Ground-state J, L, and S quantum numbers for the (**a**) transition metal, TM^{2+}, and (**b**) rare earth, RE^{3+}, ions.

Table 1. Ground-State Multiplets of Common TM and RE Ions (Van Vleck, 1932)

	Ion	S	L	J	n_{eff}			
					Term	$g[J(J+1)]^{1/2}$	Observed	$g[S(S+1)]^{1/2}$
d-Shell electrons								
1	Ti^{3+}, V^{4+}	$\frac{1}{2}$	2	$\frac{3}{2}$	$^2D_{3/2}$	1.55	1.70	1.73
2	V^{3+}	1	3	2	$^3F_2$	1.63	2.61	2.83
3	V^{2+}, Cr^{3+}	$\frac{3}{2}$	3	$\frac{3}{2}$	$^4F_{3/2}$	0.77	3.85	3.87
4	Cr^{2+}, Mn^{3+}	2	2	0	$^5D_0$	0	4.82	4.90
5	Mn^{3+}, Mn^{3+}	$\frac{3}{2}$	0	$\frac{5}{2}$	$^5S_{5/2}$	5.92	5.82	5.92
6	Fe^{2+}	2	2	4	$^5D_4$	6.7	5.36	4.90
7	Co^{2+}	$\frac{3}{2}$	3	$\frac{9}{2}$	$^4F_{9/2}$	6.63	4.90	3.87
8	Ni^{2+}	1	3	4	$^3F_4$	5.59	3.12	2.83
9	Cu^{2+}	$\frac{1}{2}$	2	$\frac{5}{2}$	$^2D_{5/2}$	3.55	1.83	1.73
10	Cu^{+}, Zn^{2+}	0	0	0	$^1S_0$	0	0	0
f-Shell electrons								
1	Ce^{3+}	$\frac{1}{2}$	3	$\frac{5}{2}$	$^2F_{5/2}$	2.54	2.51	
2	Pr^{3+}	1	5	4	$^3H_4$	3.58	3.56	
3	Nd^{3+}	$\frac{3}{2}$	6	$\frac{9}{2}$	$^4I_{9/2}$	3.62	3.3	
4	Pm^{3+}	2	6	4	$^5I_4$	2.68	—	
5	Sm^{3+}	$\frac{5}{2}$	5	$\frac{5}{2}$	$^6H_{5/2}$	0.85 (1.6)	1.74	
6	Eu^{3+}	3	3	0	$^7F_0$	0 (3.4)	3.4	
7	Gd^{3+}, Eu^{3+}	$\frac{5}{2}$	0	$\frac{5}{2}$	$^8S_{7/2}$	7.94	7.98	
8	Tb^{3+}	3	3	6	$^7F_6$	9.72	9.77	
9	Dy^{3+}	$\frac{5}{2}$	5	$\frac{15}{2}$	$^6H_{15/2}$	10.63	10.63	
10	Ho^{3+}	2	6	8	$^5I_8$	10.60	10.4	
11	Er^{3+}	$\frac{3}{2}$	6	$\frac{15}{2}$	$^4I_{15/2}$	9.59	9.5	
12	Tm^{3+}	1	5	6	$^3H_6$	7.57	7.61	
13	Yb^{3+}	$\frac{1}{2}$	3	$\frac{7}{2}$	$^2F_{7/2}$	4.53	4.5	
14	Lu^{3+}, Yb^{3+}	0	0	0	$^1S_0$	0	—	

only, the gyromagnetic factor is $g = 2$, and the single electron dipole moment is

$$\mu = \pm g\frac{e}{2m}\frac{\hbar}{2} = \pm\frac{\hbar e}{2m}, \qquad \pm g\frac{e}{2mc}\frac{\hbar}{2} = \frac{\hbar e}{2mc} \tag{18a}$$

$$\mu = \pm g\frac{e}{2m}\frac{\hbar}{2} \text{ or } \pm g\frac{e}{2mc}\frac{\hbar}{2} \tag{18b}$$

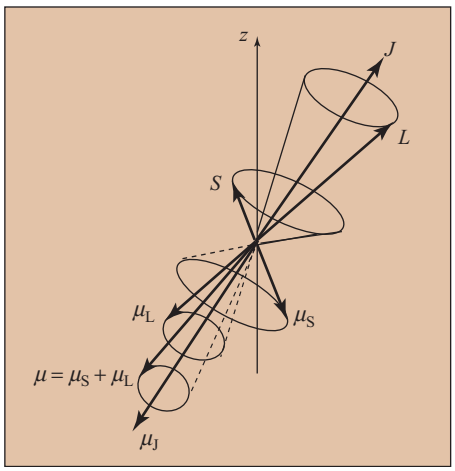

Figure 3. Vector (analogous to planetary orbit) model for the addition of angular momentum with spin angular momentum precessing around the orbital moment that precesses about the total angular momentum vector. z is the field axis (axis of quantization).

Thus, $\mu = \pm\mu_B$ with

$$\mu_B = 9.27 \times 10^{-24}\ \text{Am}^2\ (\text{J/T}) \text{ or } 9.27 \times 10^{-21}\ \text{erg/G} \tag{18c}$$

For a multielectron atom, the total spin angular momentum is

$$S = \sum_{i=1}^{n} (m_s)_i \hbar$$

with the sum over electrons in the outer shell. Hund's rules determine the occupation of eigenstates of S. The first states that for an open shell multielectron atom we fill the $(2l+1)$-fold degenerate (for d electrons $l = 2$, $(2l+1) = 5$) orbital angular momentum states so as to maximize total spin. To do so, we must fill each of the five d states with a positive (spin-up) spin before returning to fill the negative (spin-down) spin. The total spin angular momentum for 3d transition metal ions is summarized in Table 2. The dipole moments are all integral numbers of Bohr magnetons allowing for simplification of the analysis of the magnetization of ferrites that typically have quenched angular momentum.

Atomic Dipole Moments—Energy Band Theory

In systems with significant atomic overlap of the electron wave functions for orbitals responsible for magnetic dipole moments, the energy and angular momentum

Table 2. Transition Metal Ion Spin and Dipole Moments ($L=0$)

d Electrons	Cations	S	$\mu\,(\mu_B)$
1	Ti^{3+}, V^{4+}	$\frac{1}{2}$	1
2	V^{3+}	1	2
3	V^{2+}, Cr^{3+}	$\frac{3}{2}$	3
4	Cr^{2+}, Mn^{3+}	2	4
5	Mn^{2+}, Fe^{3+}	$\frac{5}{2}$	5
6	Fe^{2+}	2	4
7	Co^{2+}	$\frac{3}{2}$	3
8	Ni^{2+}	1	2
9	Cu^{2+}	$\frac{1}{2}$	1
10	Cu^{+}, Zn^{2+}	0	0

states for these electrons are no longer discrete. Instead energy levels[4] form a continuum of states over a range of energies called an *energy band*. The distribution function for these energy levels is called the *density of states*. The density of states (per unit volume), $g(\varepsilon)$, is formally defined such that the quantity $g(\varepsilon)d\varepsilon$ represents the number of electronic states (per unit volume) in the range of energies from ε to $\varepsilon + d\varepsilon$:

$$g(\varepsilon)d\varepsilon = \frac{1}{V}\frac{dN_e}{d\varepsilon}d\varepsilon \tag{19}$$

Note that this definition is not specific to the free electron model.

Figure 4a shows the density of states for free electrons with its characteristic $\varepsilon^{1/2}$ energy dependence. Many other forms (shapes) for $g(\varepsilon)$ are possible given different solutions to Schrodinger's equation with different potentials. The quantity $g(\varepsilon)d\varepsilon$ is viewed as an electronic state distribution function.

Implicit in the free electron theory is the ignoring of potential energy and therefore its influence on angular momentum. With more realistic potentials, we can calculate densities of states whose shape is influenced by the orbital angular momentum. To first approximation (and a relatively good approximation for transition metals), the orbital angular momentum can be considered to be quenched and we concern ourselves only with spin angular momentum. The formal definition is general while an $\varepsilon^{1/2}$ dependence results from the assumptions of the free electron model.

In magnetic systems we are often interested in the influence of an applied or internal (exchange) field on the distribution of energy states. Figure 4b shows the density of states for free electrons where the spin degeneracy is broken by a *Zeeman energy* due to an applied or internal (exchange) field. We divide the density of states, $g(\varepsilon)d\varepsilon$, by two, placing half the electrons in *spin-up states* and the other half in *spin-down states*. Spin-up electrons have potential energy lowered by $-\mu_B H$, where H is an applied, H_a, or internal exchange, H_{ex}, field. Spin-down electrons have their potential energy increased by $\mu_B H$.

[4] We use ε to denote the energy per electron and not the total energy which would be integrated over all electrons.

We integrate each density of states separately to yield a different number of electrons per unit volume in spin-up and spin-down bands, respectively:

$$n_\uparrow = \frac{N_\uparrow}{V} = \int_0^{\varepsilon_F} g_\uparrow(\varepsilon)d\varepsilon, \qquad n_\downarrow = \frac{N_\downarrow}{V} = \int_0^{\varepsilon_F} g_\downarrow(\varepsilon)d\varepsilon \tag{20}$$

The magnetization, net dipole moment per unit volume, is then very simply

$$M = (n_\uparrow - n_\downarrow)\mu_B \tag{21}$$

To calculate the thermodynamic properties of transition metals, one can calculate electronic structure and total energies using state-of-the-art local density functional theory. The total energy of a crystal can be calculated self-consistently and a potential function determined from the variation of the total energy with interatomic spacing. From the potential curve the equilibrium lattice spacing, the bulk modulus, cohesive energy, compressibility, etc., can be determined. $g(\varepsilon)$ is generated at the equilibrium separation describing the ground-state electronic structure. Spin-polarized calculations can be performed to determine magnetic properties. With increasing computational power and more sophisticated algorithms, it is possible to calculate these quantities accurately. Nevertheless, it is useful to have approximate analytic models for describing properties such as this or the *Friedel model*.

Pauli paramagnetism is a weak magnetism that is associated with the conduction electrons in a solid.

Pauli paramagnetism does not involve permanent local dipole moments that gave rise to the Curie law. Instead it involves a magnetic moment that is caused by the application of a field. We now describe the electronic density of states in a field.

The free electron density of states specifically accounts for a spin degeneracy of two. If we instead defined a spin-up and spin-down density of states with identical degenerate states as illustrated in Figure 4a, as in the Zeeman effect, the spin degeneracy is lifted in a field and for a free electron metal we assume the spin-up states to be rigidly shifted by an amount, $-\mu_B H$, where H is the applied field and μ_B is the spin dipole moment. Similarly the spin-down states are rigidly shifted by an energy equal to $+\mu_B H$. Now the Fermi energy of electrons in the spin-up and spin-down bands must remain the same so we remember that

$$n_\uparrow = \frac{N_\uparrow}{V} = \int_0^{\varepsilon_F} g_\uparrow(\varepsilon)d\varepsilon, \qquad n_\downarrow = \frac{N_\downarrow}{V} = \int_0^{\varepsilon_F} g_\downarrow(\varepsilon)d\varepsilon$$

and $n_\uparrow + n_\downarrow = n$ is the electron density. The magnetization, M, is $M = (n_\uparrow - n_\downarrow)\mu_B$.

We determine the T-dependent magnetic susceptibility, $\chi(T)$, by performing a Taylor series expansion of the density of states in the presence of a perturbing field:

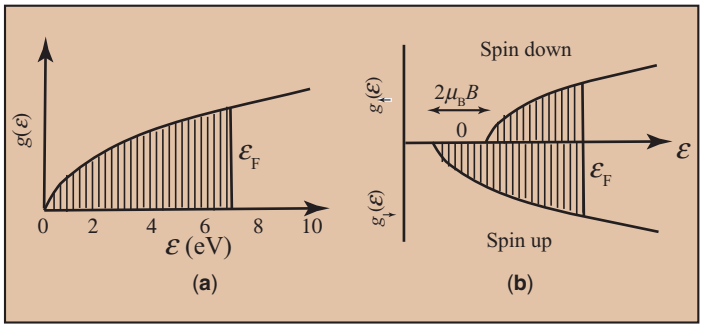

Figure 4. (**a**) Free electron density of states and (**b**) free electron density of states where the spin degeneracy is broken by a Zeeman energy due to an applied or internal (exchange) field.

$$g_{\uparrow}(\varepsilon, H) = g(\varepsilon + \mu_B H) = g(\varepsilon) + \mu_B H \frac{\partial g}{\partial \varepsilon} \tag{22}$$

$$g_{\downarrow}(\varepsilon, H) = g(\varepsilon - \mu_B H) = g(\varepsilon) - \mu_B H \frac{\partial g}{\partial \varepsilon} \tag{23}$$

and therefore

$$M = (n_{\uparrow} - n_{\downarrow})\mu_B = \frac{\mu_B}{2}\left[\int_0^{\varepsilon_F} (g(\varepsilon) + \mu_B H \frac{\partial g}{\partial \varepsilon}) d\varepsilon \right.$$
$$\left. - \int_0^{\varepsilon_F} (g(\varepsilon) - \mu_B H \frac{\partial g}{\partial \varepsilon}) d\varepsilon\right] = \mu_B^2 H \int_0^{\varepsilon_F} \left(\frac{\partial g}{\partial \varepsilon}\right) d\varepsilon = \mu_B^2 H g(\varepsilon_F)$$

and

$$\chi = \mu_B^2 g(\varepsilon_F) \tag{24}$$

which is essentially invariant with temperature. So unlike local moment paramagnetism that obeys the Curie law, with a strong $\frac{1}{T}$ dependence, free electron (Pauli) paramagnetism is nearly T independent.

A *band theory of ferromagnetism* can also be expressed in free electron theory. Building on the theory of Pauli paramagnetism, band theory considers exchange interactions between spin-up and spin-down electrons whereby electrons with parallel spins have a lower energy by $-V_{ex}$ than antiparallel spins (i.e., $V = 0$). With $B = 0$, the total energy is unstable with respect to exchange splitting when

$$V_{ex} > \frac{4\varepsilon_F}{3N} \tag{25}$$

This *Stoner criterion* determines when a system will have a lower energy with a spontaneous magnetization (ferromagnetic) than without (paramagnetic). This free electron ferromagnetism is called *itinerant ferromagnetism*. Topologically close-packed alloys can have electronic structures with sharp peaks in the density of states near the Fermi level. These peaks allow the materials to satisfy the Stoner criterion. This explains itinerant ferromagnetism observed in the Laves phase, $ZrZn_2$.

The *Friedel model* for transition metal alloys also describes the d electron density of states in transition metals (Harrison, 1989). The d states are generally more localized and atomic-like, especially for the late transition metals with more filling of the d shells. The Friedel model assumes that the density of states for d electron bands can be approximated by a constant density of states over a bandwidth, W. This is equivalent to smoothing the more complicated density of states and parameterizing it in terms of the constant $g(\varepsilon)$ and the bandwidth, W. This approximation will serve us quite well in our approximate description of the electronic structure of transition metals. Friedel's model considers contributions to the density of states of transitions metals due to the constant d electron density of states and the free electron s states. The d density of states (Fig. 4a) is centered at ε_d with a bandwidth, W_d, that is:

$$g(\varepsilon)d\varepsilon = \frac{10}{W_d}, \qquad \varepsilon_d - \frac{W_d}{2} < \varepsilon < \varepsilon_d + \frac{W_d}{2},$$

$$g(\varepsilon)d\varepsilon = 0 \quad \text{otherwise} \tag{26}$$

and we see that integrating $g(\varepsilon)d\varepsilon$ over the entire range from $\varepsilon_d - \frac{W_d}{2}$ to $\varepsilon_d + \frac{W_d}{2}$ accounts for all 10 of the d electrons. The s electron DOS begins at $\varepsilon = 0$ and ends at the Fermi level, $\varepsilon = \varepsilon_F$, and obeys the functional dependence $g_s(\varepsilon) = C\varepsilon^{1/2}$.

The Fermi level is determined by superimposing the two densities of states and filling to count the total number of electrons. Note that the atomic d and s electron count usually is not conserved (but of course the total must be). In the solid state we can use N_d and N_s to designate the integrated number of d and s electrons, respectively, such that

$$N_d = \int_{-W_d/2}^{\varepsilon_F} g_d(\varepsilon)d\varepsilon = \int_{-W_d/2}^{(-W_d/2)+(N_d W_d/10)} \frac{10}{W_d} d\varepsilon,$$

$$N_s = \int_0^{\varepsilon_F} g_s(\varepsilon)d\varepsilon \tag{27}$$

A *ferromagnetic Friedel model* considers spin-up and spin-down d bands shifted rigidly by an amount $+\Delta$ with respect to the original nonmagnetic configuration (Fig. 5b). Since the magnetism observed in transition metals is predominantly determined by more localized d electrons, the Friedel model will give more illustrative results than the free electron model. Consider the idealized density of states shown above in which a transition metal d band is modeled with a constant density of states and the s band with a free electron density of states. The atomic configuration for these atoms is given by $d^{n-2}s^2$ and $N_d = n-2$.

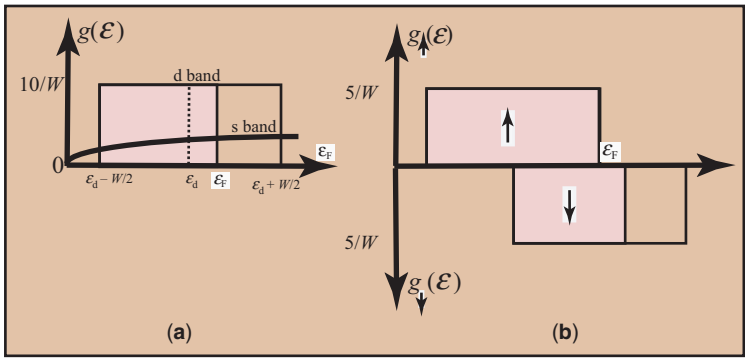

Figure 5. (**a**) Transition metal d and s band densities of states for the Friedel model and (**b**) for a spin-polarized Friedel model (d band only).

For solids, the s electrons are counted by integrating the DOS and $N_d = n - N_s$. A rough estimate approximates that $N_s \sim 0.6$ so the d count is usually higher. The average magnetic moment as a function of composition predicted by the Friedel model gives *Slater–Pauling curve* and alloy dipole moment data. Weak solutes, with a valence difference $\Delta Z \leq 1$, are explained by a *rigid band model*. A *virtual bound state* (*VBS*) model is employed when the solute perturbing potential is strong, $\Delta Z \geq 2$.

In dilute alloys, solute atoms that are only weakly perturbing (i.e., having a valency difference $\Delta Z \leq 1$), a rigid band model can be employed to explain alloying effects on magnetic moment. Rigid band theory assumes that d bands do not change much in alloys but just get filled or emptied depending on composition (Fig. 5). In this model, the magnetic moment of the solvent matrix remains independent of concentration. At the site of a solute atom the locally mobile minority-spin electrons are responsible for ensuring that the solute nuclear charge is exactly screened; thus, a moment reduction of $\Delta Z \mu_B$ is to be expected at the solute site. The average magnetic moment per solvent atom is the concentration-weighted average of that of the matrix and solute:

$$\mu = \mu_{\text{matrix}} - \Delta Z C \mu_B \qquad (28)$$

where C is the solute concentration and ΔZ is the valency difference between solute and solvent atoms. This is the basis for explaining the Slater–Pauling curve (Fig. 6) (Slater, 1937; Pauling, 1938). Figure 6b shows a more sophisticated band structure determination of the Slater–Pauling curve for FeCo alloys. Figure 6b shows the band theory prediction of the average (spin-only) dipole moment in FeCo to be in good quantitative agreement with the experimentally derived Slater–Pauling curve.

For transition metal impurities that are strongly perturbing, Friedel (1958) has proposed a *VBS* model to explain departure from the simple relationship for the compositional dependence of dipole moment above. In this case the change in average magnetic moment and suppression are predicted to be

$$\mu = \mu_{\text{matrix}} - (\Delta Z + 10) C \mu_B, \qquad \frac{d\mu}{dC} = -(\Delta Z + 10)\mu_B \quad (29)$$

Figure 7a shows the binary FeCo phase diagram. Figure 7b and c shows spin-resolved densities of states for Co and Fe atoms, in an equiatomic FeCo alloy, as a function of energy (where the Fermi energy, ε_F, is taken as the zero of energy). The number of spin-up and spin-down electrons in each band is calculated by integrating these densities of states as are the atom-resolved magnetic dipole moments. Knowledge of atomic volumes allows for the direct calculation of the alloy magnetization.

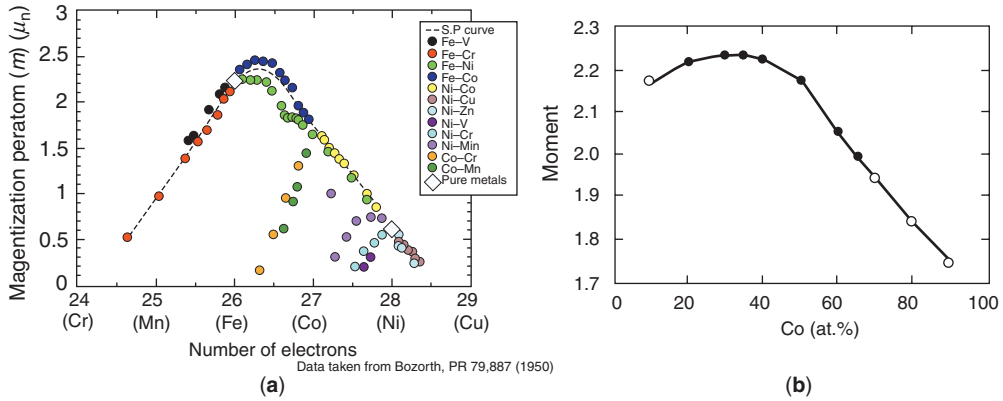

Figure 6. (**a**) Slater–Pauling curve for Fe alloys and (**b**) spin-only Slater–Pauling curve for an ordered Fe–Co alloy as determined from LKKR band structure calculations (MacLaren et al., 1999).

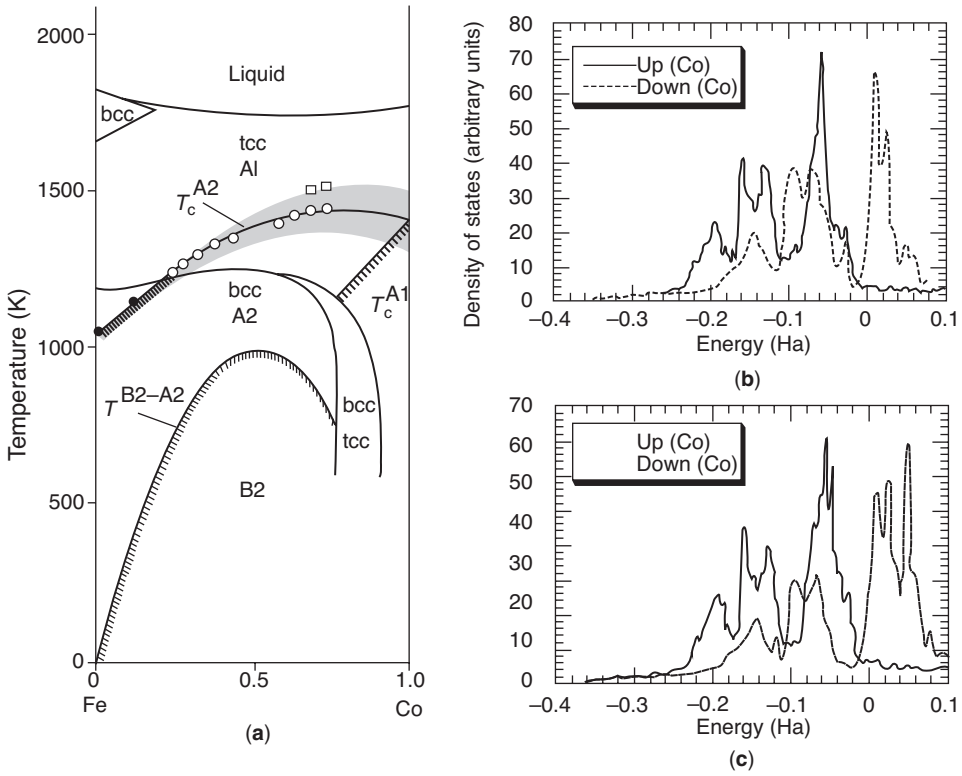

Figure 7. Binary FeCo phase diagram (**a**), and spin- and atom-resolved densities of states for an FeCo equiatomic alloy: (**b**) spin up and (**c**) spin down.

There has been considerable growth in the field of interfacial, surface, and multilayer magnetism (MacLaren et al.,1990; McHenry et al.,1990). Fundamental interest in these materials stems from predictions of enhanced local moments and phenomena associated with two-dimensional (2D) magnetism. Technological interest in these lies in their potential importance in thin film recording, spin electronics, etc. For a magnetic monolayer as a result of reduced magnetic coordination the magnetic d states become more localized and atomic-like, often causing the moment to grow since the exchange interaction greatly exceeds the bandwidth. This behavior is mimicked in buried (sandwiched) single layers or in multilayers of a magnetic species and a noninteracting host. Transition metal/noble metal systems are examples of such systems (McHenry and MacLaren, 1991).

Magnetization and Dipolar Interactions

We now turn to the definition of the magnetization, *M*. *This is the single most important concept in the chapter!*

Magnetization, *M*, is the net dipole moment per unit volume.

It is expressed as

$$M = \frac{\Sigma_{\text{atoms}} \times \mu_{\text{atom}}}{V} \tag{30}$$

where V is the volume of the material.[5] Magnetization is an extrinsic material property that depends on the constituent atoms in a system, their respective dipole moments, and how the dipole moments add together. Because dipole moments are vectors, even if they are collinear, they can add or subtract depending on whether they are parallel or antiparallel. This can give rise to many interesting types of collective magnetism.

A *paramagnet* is a material where permanent local atomic dipole moments are aligned randomly.

In the absence of an applied field, H_a, the magnetization of a paramagnet is precisely zero since the sum of randomly oriented vectors is zero. This emphasizes the importance of the word "net" in the definition of magnetization. A permanent nonzero magnetization does not necessarily follow from having permanent dipole moments. It is only through a coupling mechanism that acts to align the dipoles in the absence of a field that a macroscopic magnetization is possible.

Two dipole moments interact through dipolar interactions that are described by an interaction force analogous to the Coulomb interaction between charges. If we consider two coplanar (*xy* plane) magnetic dipole moments (Fig. 8a), $\vec{\mu}_1$ and $\vec{\mu}_2$, separated by a distance

[5] Magnetization can also be reported as specific magnetization, which is net dipole moment per unit weight.

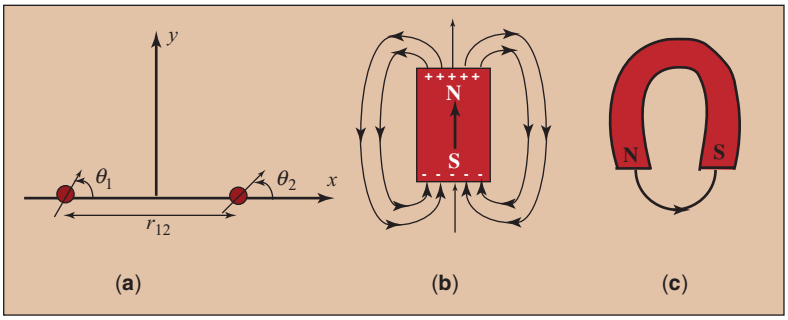

Figure 8. (**a**) Geometry of two coplanar dipole moments used to define dipolar interactions, (**b**) net surface dipole moments at the poles of a permanent magnet with a single domain, and (**c**) flux return path for magnetic dipoles in a horseshoe magnet.

r_{12} where the first dipole moment is inclined at an angle θ_1 with respect to the position vector $\vec{r}_{12}$ and the second at an angle θ_2, then the field components of field components $\vec{\mu}_1$ due to $\vec{\mu}_2$ acting at $\vec{\mu}_1$ can be written as

$$H_{1x} = \frac{-\mu_2}{4\pi\mu_0}\frac{2\cos\theta_2}{r_{12}^3}, \qquad H_{1x} = -\mu_2\frac{2\cos\theta_2}{r_{12}^3} \tag{31a}$$

$$H_{1y} = \frac{\mu_2}{4\pi\mu_0}\frac{\sin\theta_2}{r_{12}^3}, \qquad H_{1y} = \mu_2\frac{\sin\theta_2}{r_{12}^3} \tag{31b}$$

and a similar expression follows for the field components $\vec{\mu}_2$ due to $\vec{\mu}_1$ acting at $\vec{\mu}_2$. In general, the interaction potential energy between the two dipoles is given by

$$U_\mathrm{p} = \frac{1}{4\pi\mu_0 r_{12}^3}((\vec{\mu}_1\cdot\vec{\mu}_2) - \frac{3}{r_{12}^2}(\vec{\mu}_1\cdot\vec{r})(\vec{\mu}_2\cdot\vec{r})) \quad \text{(SI)} \tag{32a}$$

$$U_\mathrm{p} = \frac{1}{r_{12}^3}((\vec{\mu}_1\cdot\vec{\mu}_2) - \frac{3}{r_{12}^2}(\vec{\mu}_1\cdot\vec{r})(\vec{\mu}_2\cdot\vec{r})) \quad \text{(cgs)} \tag{32b}$$

which for collinear dipoles pointing in a direction perpendicular to $\vec{r}_{12}$ reduces to

$$E_\mathrm{p} = \frac{\pm\mu_1\mu_2}{4\pi\mu_0 r_{12}^3}, \qquad E_\mathrm{p} = \frac{\pm\mu_1\mu_2}{r_{12}^3} \tag{32c}$$

which is the familiar Coulomb's law.[6]

Like net charge in a conductor, free dipoles collect at surfaces to form the North and South Poles of a magnet (Fig. 8b). Magnetic flux lines travel from the N to the S pole of a permanent magnet. This causes a self-field, the *demagnetization field*, H_d, outside of the magnet. H_d can act to demagnetize a material for which the magnetization is not strongly tied to an *easy magnetization direction* (*EMD*). This allows us to distinguish between a *soft magnet* and a *hard magnet*.

Most hard magnets have a large *magnetocrystalline anisotropy* that acts to strongly fix the magnetization vector along particular crystal axes. As a result, they are difficult to demagnetize. A soft magnet can be used as permanent magnet, if its shape is engineered to limit the size or control the path of the demagnetization field to not interact with the magnetization vector. Fe is an example of a soft magnetic material with a large magnetization. To use Fe as a permanent magnet it is often shaped into a *horseshoe magnet* (Fig. 8c) where the return path for flux lines is spatially far from the material's magnetization.

[6] Some authors (Cullity and Graham, 2009, e.g.) use p to denote dipole moment.

Magnetization in Superconductors

The superconducting state is a state of a material in which it has no resistance to the flow of an electric current. The discovery of superconductivity by Onnes (1911) followed his successful liquification of He in 1908 (Onnes and Clay, 1908). The interplay between transport and magnetic properties in superconductors was further elucidated in the *Meissner effect* (Meissner and Ochsenfeld, 1933) (Fig. 9), where the phenomena of flux expulsion and perfect diamagnetism of superconductors were demonstrated. London (1950) gave a quantum mechanical motivation for an electrodynamic model of the superconducting wave function. This work coincided with the *Ginzburg–Landau* (*GL*) theory (Ginzburg and Landau, 1950).

The phenomenological GL theory combined an expansion of the free energy in terms of powers of the superconducting electron density (the modulus of the superconducting electron wave function) with temperature-dependent coefficients and incorporation of electrodynamic terms in the energy. The original GL theory described the intermediate state in *type I superconductors* arising from geometric (demagnetization) effects.

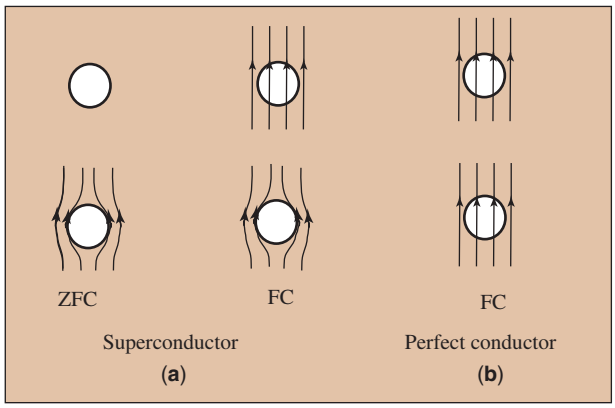

Figure 9. Flux densities for a superconductor (**a**), zero-field cooled (ZFC) or field cooled (FC) to $T < T_\mathrm{c}$, and for a perfect conductor (**b**), which is FC.

The GL theory also allowed for Abrikosov's (1957) description of the mixed state and *type II superconductivity in hard superconductors*.

A fundamental experimental manifestation of superconductivity is the Meissner effect (exclusion of flux from a superconducting material). This identifies the superconducting state as a true thermodynamic state and distinguishes it from perfect conductivity. This is illustrated in Figure 9 that compares the magnetic flux distribution near a perfect conductor and a superconductor, for conditions where the materials are cooled in a field (FC) and for cooling in zero field with subsequent application of a field (ZFC).

After cooling (ZFC) the superconductor and perfect conductor have the same response. Both the perfect conductor and superconductor exclude magnetic flux lines in the ZFC case because of diamagnetic screening currents that oppose flux changes in accordance with *Lenz's law*. The first case (FC) distinguishes a superconductor from a perfect conductor. The flux profile in a perfect conductor does not change on cooling below a hypothetical temperature where perfect conductivity occurs. However, a superconductor expels magnetic flux lines on field cooling, distinguishing it from perfect conductivity. In a clean superconductor this Meissner effect implies

$$B = 0 = H + 4\pi M \tag{33}$$

and that the magnetic susceptibility, $\chi = \frac{M}{H} = \frac{-1}{4\pi}$ for a superconductor.

Further evidence of the superconducting state as a distinct thermodynamic state is given by observation of the return to a normal resistive state for fields exceeding a *thermodynamic critical field*, $H_c(T)$, for type I superconductors. Early descriptions of the T dependence (Fig. 10) of H_c (e.g., Tuyn's law (Tuyn, 1929), $H_c(T) = H_0(1-t^2)$, where $t = \frac{T}{T_c}$) suggested the superconducting transition to be second order. Thermodynamic considerations of the Gibb's free energy density give

$$g_s = \varphi(T), \qquad g_n = \varphi(T) + \frac{H_c^2(T)}{8\pi} - \frac{H^2}{8\pi} \tag{34}$$

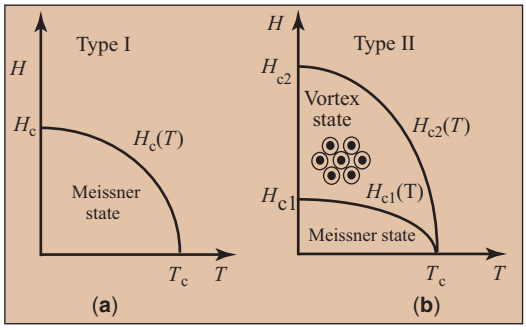

Figure 10. Critical field temperature dependence for (**a**) type I superconductor showing the thermodynamic critical field $H_c(T)$ and (**b**) type II superconductors showing the lower critical field $H_{c1}(T)$ and upper critical field $H_{c2}(T)$.

the free energies for the same material in the superconducting (type I) and normal metal states, respectively, and where the Meissner effect ($B = 0$) has been explicitly used in expressing g_s. These require that in zero field:

$$\Delta g = g_n - g_s = \frac{H_c^2(T)}{8\pi} \tag{35}$$

These free energy densities imply a latent heat for the superconducting transition:

$$L = \frac{TH_c}{4\pi}\left(\frac{\partial H_c}{\partial T}\right)_{T_c} \tag{36}$$

which is less than 0. Further, the superconducting transition is second order with a specific heat difference:

$$\Delta c = c_s - c_n = \frac{T}{4\pi}\left[H_c \frac{\partial^2 H_c}{\partial T^2}\left(\frac{\partial H_c}{\partial T}\right)^2\right] \tag{37}$$

implying a specific heat jump at the transition temperature T_c:

$$\Delta c = \frac{T}{4\pi}\left(\frac{\partial H_c}{\partial T}\right)^2_{T=T_c} \tag{38}$$

Figure 10a shows the typical temperature dependence of the thermodynamic critical field for a type I superconductor.

For a type II superconductor in a zero or constant field, H_a, the superconducting phase transition is second order. A type II superconductor has two critical fields, the *lower critical field*, $H_{c1}(T)$, and *upper critical field*, $H_{c2}(T)$. On heating, a type II superconductor, in a field, $H_a < H_{c1}$ (0K), a transition is observed both from the Meissner to the mixed state and from the mixed to the normal states at temperatures T_1 ($H_a = H_{c1}$) and T_2 ($H_a = H_{c2}$). Since $\frac{dM}{dH} = \infty$ at $H_a = H_{c1}$, it can be shown that the entropy changes continuously at approaching T_1 from below. The entropy has an infinite temperature derivative in the mixed state, that is, approaching T_1 from above. The second-order transition at $H_{c1}(T_1)$ manifests itself in a λ-type specific heat anomaly. As the temperature is further increased to T_2 (i.e., $H_a = H_{c2}(T_2)$) the entropy in the mixed state increases with increasing T and a specific heat jump is observed at T_2 consistent with a second-order phase transition. Only a single transition is observed at H_{c2} if the constant applied field exceeds H_{c1} (0 K).

The equilibrium magnetization (M vs. H) curve, shown in Figure 11a, for a type I superconductor reflects the Meissner effect slope, $\frac{-1}{4\pi}$ in the superconducting state, and the diamagnetic moment disappearing above H_c. The Meissner effect provides a description of the magnetic response of a type I superconductor, for $H < H_c$, only for long cylindrical geometries with H parallel to the long axis. For cylinders in a transverse field or for

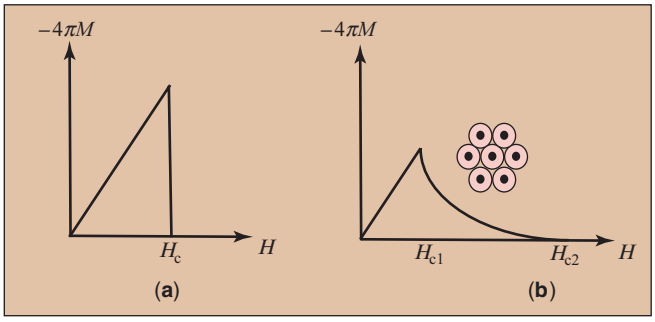

Figure 11. Equilibrium $M(H)$ curves for (**a**) type I and (**b**) type II superconductors.

noncylindrical geometries demagnetization effects need to be considered. The internal field and magnetization can be expressed as

$$H_i = H_a - DM, \qquad M = \frac{-1}{4\pi(1-D)}H \tag{39}$$

where D is the demagnetization factor ($\frac{1}{3}$ for a sphere, $\frac{1}{2}$ for a cylinder or infinite slab in a transverse field, etc.).

For noncylindrical geometries, demagnetization effects imply that the internal field can be concentrated to values that exceed H_c before the applied field H_a exceeds H_c. Since the field energy density is not greater than the critical thermodynamic value, the entire superconductor is unstable with respect to breaking down into a lamellar intermediate state with alternating superconducting and normal regions (de Gennes, 1966). The intermediate state becomes possible for fields exceeding $(1-D)H_c$, for example, a superconducting sphere exists in the Meissner state for $H < \frac{2}{3}H_c$, in the intermediate state for $\frac{2}{3}H_c < H < H_c$, and in the normal state for $H > H_c$.

Observations of the equilibrium magnetization, $M(H)$, and the H–T phase diagrams of type II superconductors are different. As shown in Figure 11b, the Meissner state (perfect diamagnetism) persists only to a *lower critical field*, H_{c1}. However, superconductivity persists until a much larger *upper critical field*, H_{c2}, is achieved. The persistence of superconductivity above H_{c1} is explained in terms of a mixed state in which the superconductor coexists with quantized units of magnetic flux called *vortices* or *fluxons*. The H–T phase diagram therefore exhibits a single Meissner phase for $H < H_{c1}(T)$, a mixed state, $H_{c1} < H < H_{c2}$ in which the superconducting and normal states coexist, and the single normal state phase for $H > H_{c2}(T)$.

For applications it is important to pin magnetic flux lines. This *flux pinning* determines the *critical current density*, J_c. J_c represents the current density that frees magnetic flux lines from pinning sites (McHenry and Sutton, 1994). Studies of *high-temperature superconductors* have elucidated the crucial role played by crystalline anisotropy in determining properties. Thermally activated dissipation in *flux creep* has been identified as an important limitation for J_c. The time-dependent decay of the magnetization has been used to study the distribution of pinning energies in HTSCs (Maley et al.,1990).

Large anisotropies in layered superconductors lead to new physical models of the H–T phase diagram in HTSCs (Nelson, 1988). This includes the notions of *vortex liquid* and *vortex glass* phases (Fisher, 1989). Examples of proposed H–T phase diagrams for HTSC materials are illustrated in Figure 12. In anisotropic materials, flux pinning and J_c values are different for fields aligned parallel and perpendicular to a crystal's c-axis. The pinning of vortex pancakes is different than for Abrikosov vortices. The concept of *intrinsic pinning* has been used to describe low-energy positions for fluxons in regions between Cu–O planes (for field parallel to the (001) plane in anisotropic materials). Models based on weakly coupled pancake vortices have been proposed for fields parallel to the c-axis for layered oxides. The *vortex melting line* of Figure 12a and b is intimately related to the state of disorder as provided by flux pinning sites. Figure 12c shows schematics of intrinsic pinning and Figure 12d shows pinning of pancake vortices in an anisotropic superconductor.

COUPLING OF MAGNETIC DIPOLE MOMENTS: MEAN FIELD THEORY

Dipolar interactions are important in defining demagnetization effects. However, they are much too weak to explain the existence of a spontaneous magnetization in

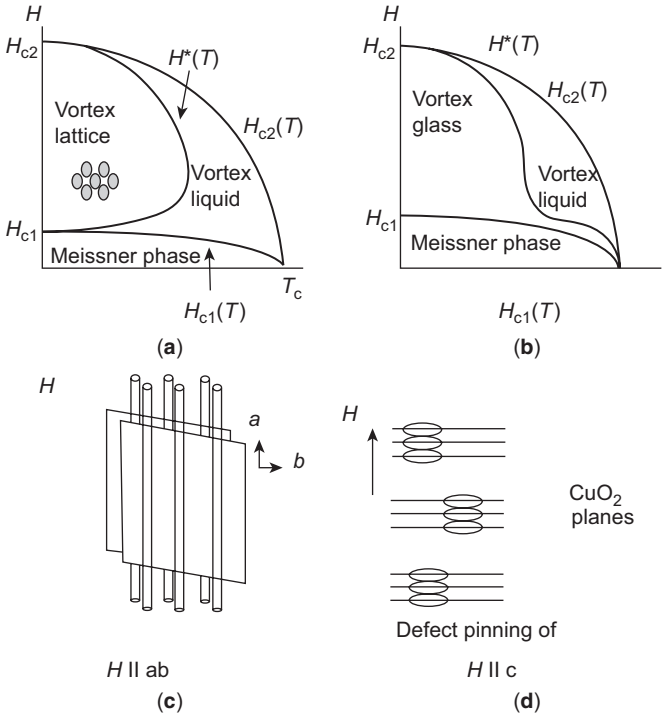

Figure 12. Vortex lattices with a melting transition for an anisotropic material with weak random pinning (**a**) and a material with strong random pinning (**b**). Schematics of intrinsic pinning (**c**) and pinning of pancake vortices (**d**) in an anisotropic superconductor.

a material at any appreciable temperature. This is because thermal energy at relatively low temperature will destroy the alignment of dipoles. To explain a spontaneous magnetization it is necessary to describe the origin of an internal magnetic field or other strong magnetic interaction that acts to align atomic dipoles in the absence of a field.

A *ferromagnet* is a material for which an *internal field* or equivalent *exchange interaction* acts to align atomic dipole moments parallel to one another in the absence of an applied field ($H = 0$).

Ferromagnetism is a *collective phenomenon* since individual atomic dipole moments interact to promote parallel alignment with one another. The interaction giving rise to the collective phenomenon of ferromagnetism has been explained by two models:

i. *Mean field theory*: considers the existence of a nonlocal internal magnetic field, called the *Weiss field*, which acts to align magnetic dipole moments even in the absence of an applied field, H_a.
ii. *Heisenberg exchange theory*: considers a local (nearest neighbor) interaction between atomic moments (spins) mediated by direct or indirect overlap of the atomic orbitals responsible for the dipole moments. This acts to align adjacent moments in the absence of an applied field, H_a.

Both of these theories help to explain the T dependence of the magnetization.

The Heisenberg theory lends itself to convenient representations of other collective magnetic phenomena such as *antiferromagnetism, ferrimagnetism, helimagnetism*, etc., illustrated in Figure 13.

An *antiferromagnet* is a material for which dipoles of equal magnitude on adjacent nearest neighbor atomic sites (or planes) are arranged in an antiparallel fashion in the absence of an applied field.

Antiferromagnets also have zero magnetization in the absence of an applied field because of the vector cancellation of adjacent moments. They exhibit temperature-dependent collective magnetism, though, because the arrangement of the dipole moments is precisely ordered.

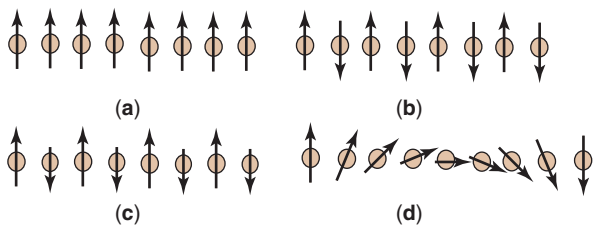

Figure 13. Atomic dipole moment configurations in a variety of magnetic ground states: (**a**) ferromagnet, (**b**) antiferromagnet, (**c**) ferrimagnet, and (**d**) noncollinear spins in a helimagnet.

A *ferrimagnet* is a material having two (or more) sublattices, for which the magnetic dipole moments of *unequal* magnitude on adjacent nearest neighbor atomic sites (or planes) are also arranged in an antiparallel fashion.

Ferrimagnets have nonzero magnetization in the absence of an applied field because their adjacent dipole moments do not cancel.[7] All of the collective magnets described thus far are *collinear magnets*, meaning that their dipole moments are either parallel or antiparallel. It is possible to have ordered magnets for which the dipole moments are not randomly arranged, but are not parallel or antiparallel. The *helimagnet* of Figure 13d is a noncollinear ordered magnet. Other examples of noncollinear ordered magnetic states include the triangular spin arrangements in some ferrites (Yafet and Kittel, 1952).

Classical and Quantum Theories of Paramagnetism

The phenomenon of *paramagnetism* results from the existence of permanent magnetic dipole moments on atoms. We have shown that in the absence of a field, a permanent atomic dipole moment results from incomplete cancellation of the electron's angular momentum vector.

In a paramagnetic material in the absence of a field, the local atomic moments are uncoupled.

For a collection of atoms, in the absence of a field, these atomic moments will be aligned in random directions so that $\langle \vec{\mu}_{atom} \rangle = 0$[8] and therefore $M = 0$. We now wish to consider the influence of an applied magnetic field on these moments. Consider the induction vector, $\vec{B}$, in our paramagnetic material arising from an applied field vector, $\vec{H}$. Each individual atomic dipole moment has a potential energy[9]:

$$U_p = -\vec{\mu} \cdot \vec{B} = -\mu B \cos\theta \qquad (40a)$$

The distinction between the classical and quantum theories of paramagnetism lies in the fact that a continuum of values of θ and therefore continuous projections of $\vec{M}$ on the field axis are allowed in the classical theory. In the quantum theory only discrete θ and projected moments, μ, are allowed consistent with the quantization of angular momentum. Notice that in either case the potential

[7] Ferrimagnets are named after a class of magnetic oxides called ferrites.
[8] We will use the symbol $\langle a \rangle$ to denote the spatial average of the quantity a.
[9] This is the Zeeman energy and represents the internal potential energy for electrons in a field.

energy is minimized when local atomic moments and induction, $\vec{B}$, are parallel.

We are now interested in determining the temperature-dependent magnetic susceptibility for a collection of local atomic moments in a paramagnetic material. In the presence of an applied field, at 0K, all atomic moments in a paramagnetic material will align themselves with the induction vector, $\vec{B}$, so as to lower their potential energy, U_p. At finite temperature, however, thermal fluctuations will cause misalignment, that is, thermal activation over the potential energy barrier leading to a T dependence of the susceptibility, $\chi(T)$. To determine $\chi(T)$ for a classical paramagnet, we express the total energy of a collection of equal atomic magnetic dipole moments in SI units as

$$U_p^{tot} = \sum_{atoms,i} -\mu_{atom}(\mu_0 H)\cos\theta_i \tag{40b}$$

where θ_i is the angle between the ith atomic dipole moment and $\vec{B}$. We consider a field along the z-axis and the set of vectors $n_i = \frac{\vec{\mu}_i}{\mu}$, which are unit vectors in the direction of the ith atomic moment, to determine $\chi(T)$; we wish to discover the temperature distribution function of the angle θ_i. The probability of any particular potential energy state being occupied is given by Boltzmann statistics, in SI units as

$$p = C\exp\left[\frac{U_p}{k_B T}\right] = C\exp\left[\frac{\mu_{atom}(\mu_0 H)\cos\theta}{k_B T}\right] \tag{40c}$$

where $p = p(U_p) = p(\theta)$. As shown in Figure 14, the number of dipoles for a given θ_i at $T = 0$K and $H = 0$ is given by

$$dn = 2\pi\sin\theta\, d\theta \tag{40d}$$

since all angles are equally probable. At finite T and H:

$$dn = C\exp\left[\frac{\mu_{atom}(\mu_0 H)\cos\theta}{k_B T}\right]2\pi\sin\theta\, d\theta \tag{40e}$$

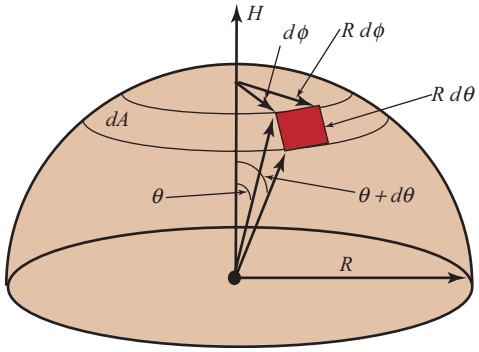

Figure 14. Distribution of moment vector angles with respect to the field axis.

and integrating

$$N = \int_0^{2\pi} dn \tag{40f}$$

gives the number of dipoles, N. We now calculate an average projected moment (along the axis of $\vec{B}$) as

$$\langle\vec{\mu}_{atom}\rangle = \frac{\int_0^{2\pi}\mu\cos\theta\, dn}{\int_0^{2\pi} dn} = \frac{\int_0^{2\pi} C\exp\left[\frac{\mu_{atom}(\mu_0 H)\cos\theta}{k_B T}\right]\mu\cos\theta\, 2\pi\sin\theta\, d\theta}{\int_0^{2\pi} C\exp\left[\frac{\mu_{atom}(\mu_0 H)\cos\theta}{k_B T}\right]2\pi\sin\theta\, d\theta} \tag{40g}$$

and using the substitution $x = \frac{\mu_{atom}\mu_0 H}{k_B T}$, we have

$$\frac{\langle\vec{\mu}_{atom}\rangle}{\mu_{atom}} = \frac{\int_0^{2\pi}\exp[x\cos\theta]\cos\theta\,\pi\sin\theta\, d\theta}{\int_0^{2\pi}\exp[x\cos\theta]\pi\sin\theta\, d\theta} \tag{40h}$$

and evaluation of the integrals reveals

$$\frac{\langle\vec{\mu}_{atom}\rangle}{\mu_{atom}} = \coth(x) - \frac{1}{x} = L(x) \tag{40i}$$

where $L(x)$ is called the Langevin function (Langevin, 1907). The Langevin function has two interesting attributes as illustrated in Figure 15:

$$\lim_{x\to\infty} L(x) = 1, \qquad \lim_{x\to 0}\frac{dL(x)}{dx} = \frac{1}{3}$$

To calculate the magnetization we remember that M is defined as the total dipole moment per unit volume (we are interested in the component of $\vec{M}$ parallel to $\vec{B}$); thus:

$$M = N_m\langle\vec{\mu}_{atom}\rangle = N_m\mu_{atom}L(x) \tag{41a}$$

where N_m is the number of magnetic dipoles per unit volume. In the large x limit $L(x) = 1$, and we infer that the saturation magnetization, M_s, is given by

$$M_s = N_m\mu_{atom} \tag{41b}$$

and the temperature (and field) dependence of the magnetization can be expressed as

$$\frac{M}{M_s} = L(x) \tag{41c}$$

In the low a limit (low field, high temperature), $L(x) \sim \frac{x}{3}$, and

$$M = M_s\left(\frac{\mu_0\mu_{atom}}{3k_B T}\right)\frac{H}{T} \tag{41d}$$

and

$$\chi = \frac{M}{H} = \frac{N_m\mu_0(\mu_{atom})^2}{3k_B T} = \frac{C}{T} \tag{41e}$$

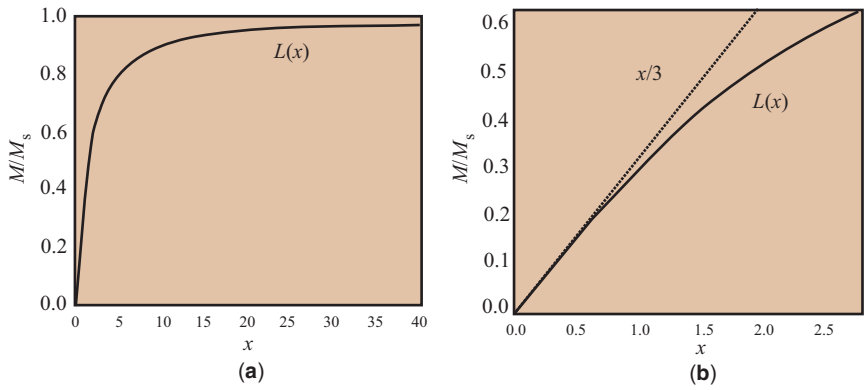

Figure 15. (**a**) Langevin function and (**b**) its low-temperature limiting form.

which is the *Curie law* of paramagnetism. Notice that if we know N_m (the concentration of magnetic atoms) from an independent experimental measurement, then an experimental determination of $\chi(T)$ allows us to solve for C (as shown in Fig. 16) as the slope of χ versus $\frac{1}{T}$ and therefore μ_{atom}. μ_{atom} is associated with the local effective moment as given by Hund's rules. In materials with a phase transition the dipoles may order below a *critical temperature*, T_c. For these the paramagnetic response is observed for $T > T_c$ and the Curie law is replaced by a *Curie–Weiss law*:

$$\chi = \frac{M}{H} = \frac{N_m \mu_0 (\mu_{atom})^2}{3k_B(T-T_c)} = \frac{C}{T-T_c}, \qquad C = \frac{N_m(\mu_{atom})^2}{3k_B} \quad \text{(cgs)} \tag{41f}$$

This ordering temperature can be associated with an internal *Weiss molecular field*, H_{int}, through the following expression:

$$T_c = \lambda C, \qquad H_{int} = \lambda M \tag{41g}$$

where λ is called the molecular field constant.

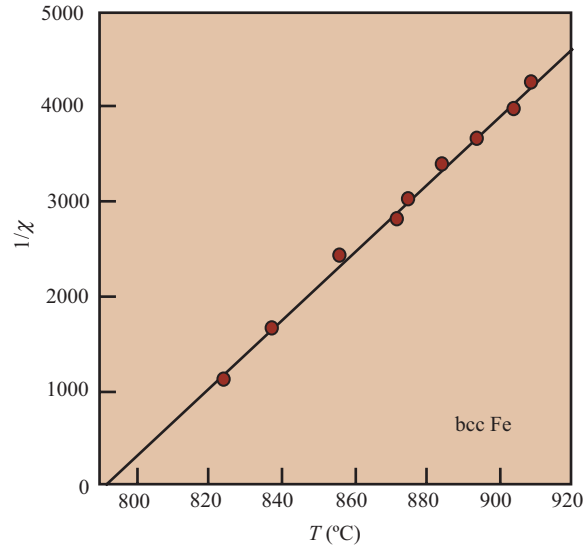

Figure 16. Curie–Weiss law fit to paramagnetic magnetization data for bcc Fe above its ordering temperature $T_c = \Theta = 794$K (measurements of Sucksmith and Pearce).

To further describe the response of the quantum paramagnet we again consider an atom left with a permanent magnetic dipole moment of magnitude $\mu_{atom} = \mu$, due to its unfilled shells. We can now consider its magnetic behavior in an applied field. The magnetic induction, $\vec{B}$, will align the atomic dipole moments. The potential energy of a dipole oriented at an angle θ with respect to the magnetic induction is

$$U_p = -\vec{\mu} \cdot \vec{B} = g\mu_B(\vec{J} \cdot \vec{B}) \tag{42a}$$

where g is the gyromagnetic factor. Now our quantum mechanical description of angular momentum tells us that $|J_z|$, the projection of the total angular momentum on the field axis, must be quantized, that is:

$$U_p = (g\mu_B)m_J B \tag{42b}$$

where $m_J = J, J-1, \ldots -J$ and $J = |\vec{J}| = |\vec{L} + \vec{S}|$ that may take on integral or half-integral values. In the case of spin only, $m_J = m_s = \pm\frac{1}{2}$. The quantization of J_z requires that only certain angles θ are possible for the orientation of $\vec{\mu}$ with respect to $\vec{B}$. The ground state corresponds to $\vec{\mu} || \vec{B}$. However, with increasing thermal energy, it is possible to misalign $\vec{\mu}$ so as to occupy excited angular momentum states. If we consider the simple system with spin only, the Zeeman splitting between the eigenstates is $\mu_B B$, the lower lying state corresponding to $m_J = m_s = -\frac{1}{2}$ with the spin moment parallel to the field. The higher energy state corresponds to $m_J = m_s = \frac{1}{2}$ and an antiparallel spin moment. For this simple two-level system we can use Boltzmann statistics to describe the population of these two states. With N isolated atoms per unit volume in a field, we define

$$N_1 = N_\uparrow = A \exp\left[\frac{\mu_B(\mu_0 H)}{k_B T}\right],$$
$$N_2 = N_\downarrow = A \exp\left[\frac{-\mu_B(\mu_0 H)}{k_B T}\right] \tag{43a}$$

Recognizing that $N = N_1 + N_2$ and the net magnetization (dipole moment/volume) is $M = (N_1 - N_2)\mu$, we have

$$M = \frac{N}{A(\exp x + \exp(-x))} \times A(\exp x - \exp(-x))\mu$$

$$= N\mu \frac{\exp x - \exp(-x)}{\exp x + \exp(-x)} = N\mu \tanh x \tag{43b}$$

where $x = \frac{\mu_B(\mu_0 H)}{k_B T}$. Notice that for small values of x, $\tanh(x) \sim x$ and we can approximate M and determine χ:

$$M = N\mu \frac{\mu_B(\mu_0 H)}{k_B T} = \frac{N\mu_B^2(\mu_0 H)}{k_B T}, \qquad \chi = \frac{M}{H} = \frac{N\mu_0\mu_B^2}{k_B T} \tag{43c}$$

The expression relating χ to $\frac{1}{T}$ is called the *paramagnetic Curie law*.

For the case where we have both spin and orbital angular momenta, we are interested in the J quantum number and the $2J+1$ possible values of m_J, each giving a different projected value (J_z) of J along the field (z) axis. In this case we no longer have a two-level system but instead a $(2J+1)$-level system. The $2J+1$ projections are equally spaced in energy. Again considering a Boltzmann distribution to describe the thermal occupation of the excited states, we find that $\vec{\mu} \cdot \vec{B} = \frac{J}{J_z}\mu_B B$ and

$$\mu = \frac{\sum_J \frac{J}{J_z}\mu_B \exp\left[\frac{J}{J_z}\frac{\mu_B(\mu_0 H)}{k_B T}\right]}{\sum_J \exp\left[\frac{J}{J_z}\frac{\mu_B(\mu_0 H)}{k_B T}\right]}, \qquad N = \sum_J \exp\left[\frac{J}{J_z}\frac{\mu_B(\mu_0 H)}{k_B T}\right] \tag{44a}$$

so that finally

$$M = N\mu = N\frac{\sum_{-J} J\frac{J}{J_z}\mu_B \exp\left[\frac{J}{J_z}\frac{\mu_B(\mu_0 H)}{k_B T}\right]}{\sum_J \exp\left[\frac{J}{J_z}\frac{\mu_B(\mu_0 H)}{k_B T}\right]} = NgJ\mu_B B_J(x) \tag{44b}$$

where $x = \frac{gJ\mu_B B}{k_B T}$ and $B_J(x)$ is called the Brillouin function and is expressed as

$$B_J(x) = \frac{2J+1}{2J}\coth\left[\frac{(2J+1)x}{2J}\right] - \frac{1}{2J}\coth\left[\frac{x}{2J}\right] \tag{44c}$$

For $J = \frac{1}{2}$, $B_J(x) = \tanh(x)$ as before. The small x expansion for $B_J(x)$ is

$$B_J(x) = \frac{x(J+1)}{3}, \quad x \ll 1 \tag{45a}$$

For small x we then see that

$$M = \frac{Ng^2(\mu_0 H)\mu_B^2 J(J+1)}{3k_B T} = \frac{Np_{\text{eff}}^2(\mu_0 H)}{3k_B T} \tag{45b}$$

where

$$p_{\text{eff}} = g[J(J+1)]^{1/2}\mu_B \tag{45c}$$

is called the effective local moment. This expression is a *Curie law* with

$$\chi = \frac{C}{T}, \qquad C = \frac{Np_{\text{eff}}^2}{3k_B T} \tag{45d}$$

The effective local moment can be contrasted with the maximum value that occurs when all of the dipoles are aligned with the magnetic field. This has the following value:

$$\mu_H = gJ\mu_B \tag{45e}$$

Experimentally derived magnetic susceptibility versus T data can be plotted as $\frac{1}{\chi}$ versus T to determine C (from the slope) and therefore p_{eff} (if the concentration of paramagnetic ions is known). Figure 17 shows the behavior of M versus $\frac{H}{T}$ for a paramagnetic material. At low temperature $M(x) \sim \frac{x}{3}$. $M(H)$ is well described by a Brillouin function with a characteristic $\frac{H}{T}$ scaling bringing curves from different temperatures into coincidence.

Mean Field Theory—Ferromagnetism

Ferromagnetic response is distinct from paramagnetic response, in that local atomic moments are coupled in the absence of an applied field. A ferromagnetic material possesses a nonzero magnetization over a macroscopic volume, called a domain, containing many atomic sites, even for $H = 0$. Ferromagnetism is a collective phenomenon since individual atomic moments interact so as to promote alignment with one another. The interaction between individual atomic moments gives rise to the collective phenomenon of ferromagnetism that can be explained in terms of *mean field theory* or *Heisenberg exchange theory*. We consider the mean field theory here and the Heisenberg exchange theory (Heisenberg, 1928) below. The two theories do lead to different pictures of certain aspects of the collective phenomena and the ferromagnetic phase transformation. The Heisenberg theory also lends itself to quite convenient representations of other collective magnetic phenomena such as antiferromagnetism, ferrimagnetism, helimagnetism, etc.

The mean field theory of ferromagnetism was introduced by Weiss (1907). Weiss postulated the existence of an *internal magnetic field* (the Weiss field), $\vec{H}_{\text{int}}$, which

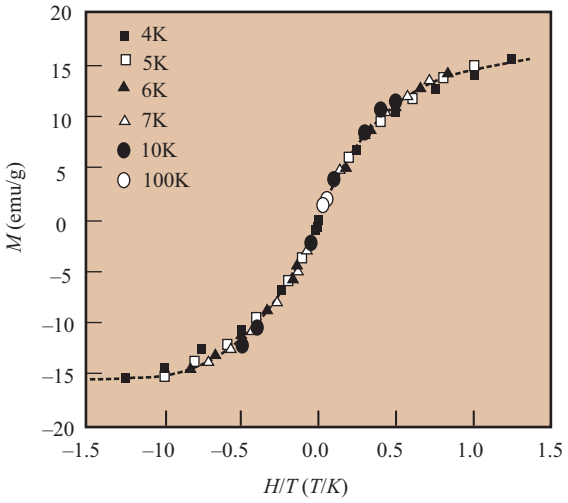

Figure 17. Paramagnetic response of Gd^{3+} ions in Gd_2C_3 nanocrystals with $\frac{H}{T}$ scaling (Diggs et al., 1994).

acts to align the atomic moments even in the absence of an external applied field, H_a. The main assumption of mean field theory is that the internal field is directly proportional to the magnetization of the sample:

$$\vec{H}_{\text{int}} = \lambda \vec{M} \tag{46a}$$

where the constant of proportionality, λ, is called the *Weiss molecular field constant* (we can think of it as a crystal field constant). We write the field quantities as vectors because it is possible to have situations in which the magnetic dipoles are noncollinear but still ordered (i.e., a helimagnet where the ordering is wave-like, or a triangular spin structure). In the cases discussed below, ferromagnetism, antiferromagnetism, and ferrimagnetism, the dipoles are collinear, either parallel or antiparallel.

We now wish to consider the effects on ferromagnetic response of application of an applied field, H_a, and the randomizing effects of temperature. We can treat this problem identically to that of a paramagnet but now considering the superposition of the applied and internal magnetic fields. By analogy we conclude that

$$\frac{\langle \vec{\mu}_{\text{atom}} \rangle}{\mu_{\text{atom}}} = \coth(x') - \frac{1}{x'} = L(x'), \qquad \frac{M}{M_s} = L(x') \tag{46b}$$

where

$$x' = \frac{\mu_0 \mu_{\text{atom}}}{k_B T}[H_a + \lambda M] \tag{46c}$$

for a collection of classical dipole moments. Similarly, $M = N_m \langle \vec{\mu}_{\text{atom}} \rangle$ and

$$\frac{M}{N_m \mu_{\text{atom}}} = \frac{M}{M_s} = L\left(\frac{\mu_0 \mu_{\text{atom}}}{k_B T}[H_a + \lambda M]\right) \tag{46d}$$

where this simple expression represents a formidable transcendental equation to solve. Under appropriate conditions, this leads to solutions for which there is a nonzero magnetization (*spontaneous magnetization*) even in the absence of an applied field. We can show this graphically considering $M(H = 0)$ defining the variables:

$$b = \frac{\mu_0 \mu_{\text{atom}}}{k_B T}[\lambda M] \tag{46e}$$

which is dimensionless (and $M(0) = M_s L(b)$) and define:

$$T_c = \frac{N_m \mu_0 (\mu_{\text{atom}})^2 \lambda}{3 k_B} \tag{46f}$$

Notice that T_c has units of temperature. Notice also that

$$\frac{b}{T_c} = \frac{3}{T}\left[\frac{M(0)}{M_s}\right] \tag{46g}$$

so that

$$\frac{M(0)}{M_s} = \frac{bT}{3T_c} = L(b) \tag{46h}$$

The reduced magnetization equations (i.e., $\frac{M(0)}{M_s} = \frac{bT}{3T_c}$ and $\frac{M(0)}{M_s} = L(b)$) can be solved graphically, for any choice of T by considering the intersection of the two functions $\frac{b}{3}\left(\frac{T}{T_c}\right)$ and $L(b)$. As is shown in Figure 18, for $T \geq T_c$ the only solutions for which the two equations are simultaneously satisfied are when $M = 0$, that is, no spontaneous magnetization and paramagnetic response. For $T < T_c$ we obtain solutions with a nonzero, spontaneous, magnetization, the defining feature of a ferromagnet. For $T = 0$ to $T = T_c$ we can determine the spontaneous magnetization graphically as the intersection of our two functions $\frac{b}{3}\left(\frac{T}{T_c}\right)$ and $L(b)$. This allows us to determine the zero-field magnetization, $M(0)$, as a fraction of the spontaneous magnetization as a function of temperature. As shown in the phase diagram of Figure 18c, $\frac{M(0,T)}{M_s}$ decreases monotonically from 1, at 0K, to 0 at $T = T_c$, where T_c is called the *ferromagnetic Curie temperature*. At $T = T_c$, we have a phase transformation from ferromagnetic to paramagnetic response that can be shown to be second order in the absence of a field. In summary, mean field theory for ferromagnets predicts:

i. For $T < T_c$, collective magnetic response gives rise to a spontaneous magnetization even in the absence of a field. This spontaneous magnetization is the defining feature of a ferromagnet.
ii. For $T > T_c$, the misaligning effects of temperature serve to completely randomize the direction of the atomic moments in the absence of a field. The loss

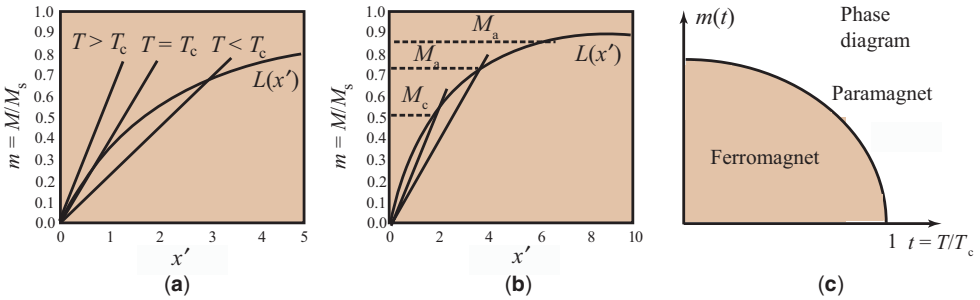

Figure 18. (**a**) Intersection between the curves $\frac{b}{3}\left(\frac{T}{T_c}\right)$ and $L(b)$ for $T < T_c$ gives a nonzero, stable ferromagnetic state and (**b**) the locus of $M(T)$ determined by intersections at temperatures $T < T_c$; (**c**) reduced magnetization, m, versus reduced temperature, $t = \frac{T}{T_c}$, as derived from (**b**).

Table 3. Structures, Room-Temperature, and 0 K Saturation Magnetizations and Curie Temperatures for Elemental Ferromagnets (O'Handley, 1987)

Element	Structure	M_s(290K) (emu/cm^3)	M_s(0K) (emu/cm^3)	$n_B(\mu_B)$	T_c (K)
Fe	bcc	1707	1740	2.22	1043
Co	hcp, fcc	1440	1446	1.72	1388
Ni	fcc	485	510	1.72	627
Gd	hcp	—	2060	7.63	292
Dy	hcp	—	2920	10.2	88

of the spontaneous magnetization defines the return to paramagnetic response.

iii. In the absence of a field, the ferromagnetic to paramagnetic phase transition is second order (first order in a field).

Table 3 summarizes structures, room-temperature, and 0K saturation magnetizations and Curie temperatures for elemental ferromagnets (O'Handley, 2000).

As a last ramification of the mean field theory we consider the behavior of magnetic dipoles in the paramagnetic state $T > T_c$ with the application of a small field, H. We wish to examine the expression for the paramagnetic susceptibility, $\chi(T) = \frac{M(H,T)}{H}$. Here again we can assume that we are in the small argument regime for describing the Langevin function so that

$$\frac{M(H,T)}{H} = L(x') = \frac{a'}{3} = \frac{\mu_0 \mu_{atom} \lambda}{3k_B T}(H + \lambda M) \tag{47a}$$

and

$$M = \frac{\left[\frac{N_m \mu_0 (\mu_{atom})^2}{3k_B}\right] H}{T - \frac{N_m \mu_0 (\mu_{atom} \lambda)^2}{3k_B}} = \frac{CH}{T - T_c} \tag{47b}$$

Thus, the susceptibility, $\chi(T)$, is described by the so-called *Curie–Weiss law*:

$$\chi = \frac{M}{H} = \frac{C}{T - T_c} \tag{47c}$$

where, as before, C is the Curie constant and T_c is the Curie temperature. Notice that

$$C = \left[\frac{N_m \mu_0 (\mu_{atom})^2}{3k_B}\right] \tag{47d}$$

It is possible to determine the atomic moment and molecular field constant from $\chi(T)$ data. Plotting $\frac{1}{\chi}$ versus T allows for determination of a slope $\left(= \frac{1}{C}\right)$, from which μ_{atom} can be determined, and an intercept $-\frac{T_c}{C} = -\lambda$. The ferromagnetic to paramagnetic phase transition is not as sharp at $T = T_c$ in a field, exhibiting a Curie tail that reflects the ordering influence of field in the high-temperature paramagnetic phase.

Mean Field Theory for Antiferromagnetism and Ferrimagnetism

Mean field theories for antiferromagnetic and ferrimagnetic ordering require expanding the internal field in terms of more than one molecular field constant, each multiplied by the magnetization due to a different sublattice. An antiferromagnet has dipole moments on adjacent atomic sites arranged in an antiparallel fashion below an ordering temperature, T_N, called the *Neel temperature*. Cr is an example of an antiferromagnet. The susceptibility of an antiferromagnet does not diverge at the ordering temperature but instead has a weak cusp. The mean field theory for antiferromagnets considers two sublattices, an A sublattice for which the spin moment is down. We can express, in mean field theory, the internal fields on the A and B sites, respectively:

$$\vec{H}_A^{int} = -\lambda_{BA}\vec{M}_B, \qquad \vec{H}_B^{int} = -\lambda_{AB}\vec{M}_A \tag{48a}$$

where by symmetry $\lambda_{BA} = \lambda_{BA}$, and $\vec{M}_A$ and $\vec{M}_B$ are the magnetizations of the A and B sublattices. The mean field theory thus considers a field at the B atoms due to the magnetization of the A atoms and vice versa. Using the paramagnetic susceptibilities χ_A and χ_B, which are the same and both equal χ_p, we can express the high-temperature magnetization for each sublattice as

$$\vec{M}_A = \chi_p(\vec{H}_a + \vec{H}_A^{int}) = \frac{C_A}{T}(\vec{H}_a - \lambda_{BA}\vec{M}_B) \tag{48b}$$

$$\vec{M}_B = \chi_p(\vec{H}_a + \vec{H}_B^{int}) = \frac{C_B}{T}(\vec{H}_a - \lambda_{AB}\vec{M}_A) \tag{48c}$$

Now for an antiferromagnet the moments on the A and B sublattices are equal and opposite so that $C_A = C_B = C$ and on rearranging we get

$$T\vec{M}_A + C\lambda_{AB}\vec{M}_B = C\vec{H}_a \tag{48d}$$

$$C\lambda_{AB}\vec{M}_A + T\vec{M}_B = C\vec{H}_a \tag{48e}$$

In the limit as $H_a \to 0$ these two equations have nonzero solutions (spontaneous magnetizations) for $\vec{M}_A$ and $\vec{M}_B$ if the determinant of the coefficients vanishes, that is:

$$\begin{vmatrix} T & \lambda C \\ \lambda C & T \end{vmatrix} = 0 \tag{48f}$$

and we can solve for the ordering temperature:

$$T_N = \lambda C \tag{48g}$$

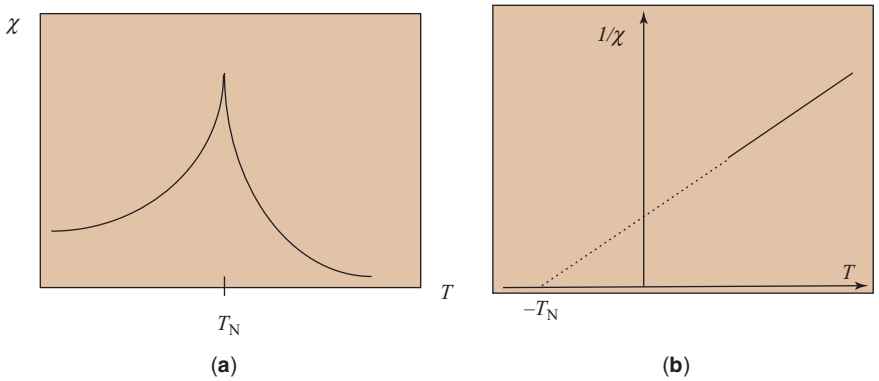

Figure 19. (**a**) T dependence of the magnetic susceptibility for an antiferromagnetic material and (**b**) inverse susceptibility as a function of T.

For $T > T_N$ the susceptibility is given by

$$\chi = \frac{2CT - 2\lambda C^2}{T^2 - (\lambda C)^2} = \frac{2C}{T + \lambda C} = \frac{2C}{T + T_N} \tag{48h}$$

Figure 19 shows that this susceptibility has a cusp at the Neel temperature. Table 4 summarizes Neel temperatures for some simple antiferromagnets (O'Handley, 2000).

Ferrites

The mean field theory for antiferromagnets is easily generalized to simple AB ferrimagnetic alloys. Here the magnitude of the moment on the A and B sublattices need not be the same and therefore $C_A \neq C_B$ in the limit as $H_a \to 0$; the determinant of the coefficients is

$$\begin{vmatrix} T & \lambda C_B \\ \lambda C_A & T \end{vmatrix} = 0 \tag{49a}$$

and the ferrimagnetic order temperature is determined to be

$$T_N = (\lambda C_A \lambda C_B)^{1/2} \tag{49b}$$

The magnetic susceptibility for $T > T_N$ becomes

$$\chi = \frac{(C_A + C_B)T - 2\lambda C_A C_B}{T^2 - T_N^2} \tag{49c}$$

with curvature in $\frac{1}{\chi}$ versus T characteristic of a ferrimagnet.

The mean field theory for spinel ferrimagnets can be even richer. In the spinel structure, magnetic cations may occupy octahedral A or tetrahedral B sites and are close enough that A–A, A–B, and B–B mean fields are possible.

Table 4. Neel Temperatures for Some Simple Antiferromagnets

Material	T_N (K)
NiO	600
Cr	311
Mn	95
FeO	198

Since the signs of all of the Weiss interactions are negative, if the A and B sites couple antiferromagnetically, then the A–A and B–B pairs align parallel.

The mean field theory of magnetic ordering in spinels considers the magnetic exchange interactions between cations. The mean field theory of ferrimagnetism can be extended to account for A–A, A–B, and B–B interactions in ferrites. The *Neel theory of two-sublattice ferrimagnetism* is used to consider A–A, A–B, and B–B interactions instead of the simple A–B interactions discussed earlier. In this case the mean field theory is expressed as

$$\vec{H}_A^{\text{int}} = -\lambda_{AA}\vec{M}_A - \lambda_{BA}\vec{M}_B, \quad \vec{H}_B^{\text{int}} = -\lambda_{AB}\vec{M}_A - \lambda_{BB}\vec{M}_B \tag{50}$$

With three mean field parameters, solutions to the mean field equations give rise to a variety of different temperature dependences for the magnetization, $M(T)$. **Louis Neel** solved the mean field equations to describe six different T dependences for the magnetization. Possible ground-state configurations for the dipole moments can be made even further complicated if one allows for *noncollinear dipole moments* (not parallel or antiparallel). This is considered in the *Yafet–Kittel theory* that describes triangular spin configurations in ferrites. Table 5 summarizes room-temperature saturation magnetizations and Neel temperatures for selected spinel ferrites (O'Handley, 1987).

EXCHANGE THEORY

Exchange is an atomic quantum mechanical phenomenon that describes the origins of the internal fields. *Heisenberg exchange theory* considers a local (nearest

Table 5. Room-Temperature Saturation Magnetizations and Neel Temperatures for Selected Spinel Ferrites (O'Handley, 2000)

Element	M_s(290K) (emu/cm^3)	n_B (μ_B)	T_N (K)
(Mn O)Fe_2O_3	410	5.0	573
(FeO)Fe_2O_3	480	4.1	858
(CoO)Fe_2O_3	—	3.2	—
(NiO)Fe_2O_3	270	2.4	858
(CuO)Fe_2O_3	135	1.3	728

neighbor) interaction between atomic moments (spins) that acts to align adjacent moments in the absence of an applied field. Various types of exchange interactions exist in materials. These can be divided into *direct exchange* and *mediated (indirect) exchange*. Direct exchange results from the direct overlap of the orbitals responsible for atomic dipole moments. Indirect exchange mechanisms include those mediated by overlap between the magnetic orbitals and nonmagnetic orbitals on the same or other species. The *superexchange mechanism* involves overlap between magnetic orbitals and the p orbitals on intervening oxygen or other anions. *RKKY interactions* are those mediated through the conduction electrons. Exchange determines the strength of the coupling between dipoles and therefore the temperature dependence of the magnetization. The term *random exchange* refers to the weakening of exchange interactions by disorder and its consequent effects on the temperature dependence of the magnetization.

Heisenberg Exchange Theory

Heisenberg exchange theory (Heisenberg, 1928) considers a local (nearest neighbor) interaction between atomic moments (spins) that acts to align adjacent moments even in the absence of a field. The Heisenberg model considers ferromagnetism and the defining spontaneous magnetization to result from nearest neighbor exchange interactions that act to align spins in a parallel configuration. The Heisenberg model can be further generalized to account for atomic moments of different magnitude, that is, in alloys, and for exchange interactions that act to align nearest neighbor moments in an antiparallel fashion or in a noncollinear relationship. Let us consider first the Heisenberg ferromagnet. Here we assume that the atomic moments on nearest neighbor sites are coupled by a nearest neighbor exchange interaction giving rise to a potential energy:

$$U_p = J_{ex}\vec{S}_i \cdot \vec{S}_{i+1} \tag{51a}$$

between identical spins at sites i and $i+1$ in a 1D lattice. For identical spins:

$$U_p = -2J_{ex}S^2 \cos\theta_{i,i+1} \tag{51b}$$

which for $J_{ex} > 0$ favors parallel spins. For a linear chain of N spins (where N is large) or exploiting *periodic, Born–Von Karmon BC*, the total internal energy is

$$U_p = -2J_{ex}S^2 \sum_{i=1}^{N} \cos\theta_{i,i+1} \tag{51c}$$

which for $J_{ex} > 0$ is minimized for a configuration in which all the spins are aligned in a parallel ferromagnetic configuration.

Combining mean field theory and the Heisenberg model, the Curie temperature can be estimated. A statistical mechanical description of exchange has been developed within the context of the *Ising model*. One of the results of this model allows us to associate the exchange interaction with the *Weiss molecular field of mean field theory*. This results in the following relationship:

$$\lambda = \frac{ZJ_{ex}}{4N\mu_0\mu_B^2} \tag{52}$$

Thus, larger exchange interactions result in higher Curie temperatures. This allows us to use the results of mean field theory to express the T dependence of the magnetization. For spin-only angular momentum this is

$$M(T) = M_0 \tanh\left[\frac{\mu_0\mu_B}{k_B T}\left(H + \frac{ZJ_{ex}M}{4N\mu_0\mu_B}\right)\right] \tag{53}$$

and similar expressions for the Langevin and Brillouin functions for classical and total angular momentum models.

Exchange interactions result from the spatially dependent energy functional for electrons with parallel or antiparallel spins (or canted spins in more complicated models). For the hydrogen molecule, for example, as shown in Figure 20a the configuration with electron spins aligned parallel is stable at larger interatomic separations and that aligned antiparallel at smaller interatomic separations. The choice of spin configuration depends on the relationship between the crossover radius and the equilibrium separation of the atoms.

The famous *Bethe–Slater curve* (Bethe and Sommerfeld, 1984; Slater, 1930) (Fig. 20b) predicts the sign of the

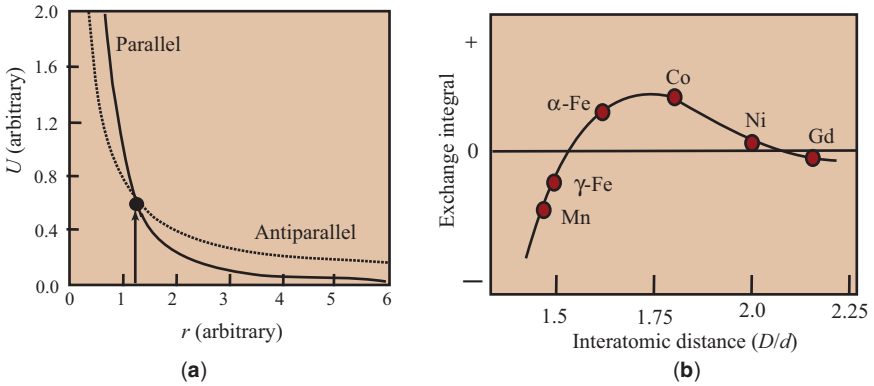

Figure 20. (**a**) Energies for parallel and antiparallel spins in the hydrogen molecule as a function of interatomic separation and (**b**) the Bethe–Slater curve predicting the sign of the exchange interaction in 3d transition metal solids (Bethe and Sommerfeld, 1984; Slater, 1930).

exchange interaction in 3d transition metal solids. The interplay between electron–electron Coulomb interactions and the constraints of the *Pauli exclusion principle* determine the sign of the exchange interaction. In transition metal solids a measure of the overlap between nearest neighbor d orbitals is given by the ratio of the atomic to the 3d ionic (or nearest neighbor) radius. The Bethe–Slater curve provides an empirical description of the exchange integral as a function of composition (or more accurately, with interatomic spacing to 3d orbital ratio). The ratio of the 3d ionic radius to the near neighbor distance describes the amount of orbital overlap (or exchange).

At this point it is useful to repeat the Heisenberg model predictions for other magnetic ground states. For example, notice that if $J_{ex} < 0$, an antiparallel configuration for adjacent spins in a 1D chain is predicted, consistent with an antiferromagnetic ground state as shown in Figure 13b. We can deduce a ferrimagnetic ground state as illustrated in Figure 13c and observed, for example, for ferrites when we have $J_{ex} < 0$ and two magnetic sublattices, for example, a and b, for which $\mu_a \neq \mu_b$. In 3D systems it is possible to relax the restrictions of nearest neighbor exchange and it is also possible to have noncollinear exchange interactions as shown in Figure 13d for a helimagnet. In certain ferrite systems (e.g., Mn_2O_3) it has been observed that Mn atoms in the octahedral and tetrahedral sites in fcc interstices of the oxygen anion sublattice couple in a Yafet–Kittel triangular spin configuration (Yafet and Kittel, 1952).

Superexchange

In the context of the ferrites and other oxides we may distinguish between direct and indirect exchange. We have described ferrimagnetic and Yafet–Kittel triangular spin configurations between neighboring magnetic cation sites. This is an example of an indirect exchange mechanism since it must be transmitted through intervening nearest neighbor oxygen sites. In fact, the exchange interaction is transmitted through overlap between magnetic d orbitals on the cation sites and the p orbitals of oxygen (Neel, 1932). This particular p orbital transmitted indirect exchange interaction is given the name superexchange and illustrated in Figure 21.

The size of superexchange interactions depends on the distance and angles of the d–p–d bonds in the crystal. These are determined by the crystallography. Figure 22

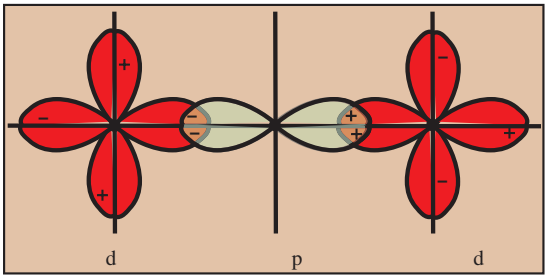

Figure 21. Superexchange interaction of magnetic cation d orbitals mediated by an O p orbital.

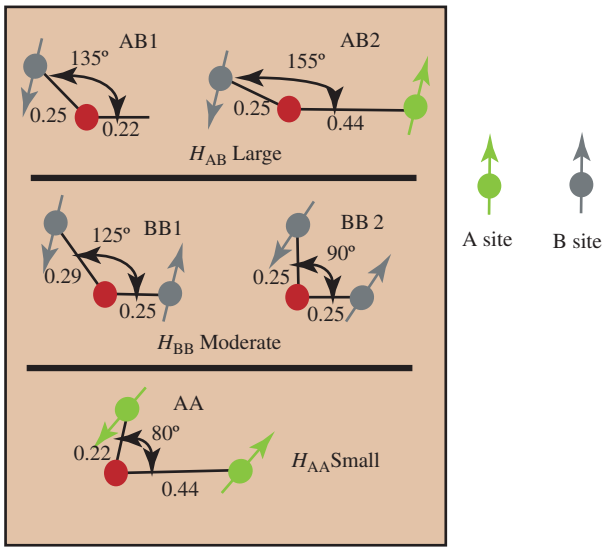

Figure 22. Geometry of the superexchange interactions in the spinel structure.

illustrates the geometry of the superexchange interactions in the spinel structure. The strongest superexchange interactions occur for bond angles approaching 180°.

RKKY Exchange

Another form of indirect exchange has recently been shown to be important in, for example, rare earth metal systems and in magnetic/nonmagnetic multilayers. This exchange is the oscillatory RKKY exchange (Fig. 23a) (Ruderman and Kittel, 1954; Kasuya, 1984; Yosida, 1957) that is mediated through the conduction electron gas often associated with nonmagnetic atoms but sometimes associated, for example, with sp conduction electrons of the magnetic atoms in rare earths. This indirect exchange is transmitted by polarization of the free electron gas. The free electron sea can be characterized by a wavevector called the Fermi wavevector that is defined as

$$k_F = \left[\frac{3\pi^2 N}{V}\right]^{1/3} \tag{54}$$

where $\frac{N}{V}$ is the number of free electrons per unit volume.

Examples of magnetic systems coupling through RKKY interactions include the rare earths. In these the Hund's rule ground state is determined by 4f electrons that are very localized, that is, close to the nucleus and shielded by conduction electrons. Therefore, there is no direct exchange since 4f states do not overlap from site to site. Instead coupling occurs through free electrons. 4f dipole moments in rare earth elements polarize the free electrons around them; these in turn communicate the information to 4f dipole moments on adjacent sites. Coupling through the conduction electrons is influenced by *Friedel oscillations* in the conduction electron spin density.

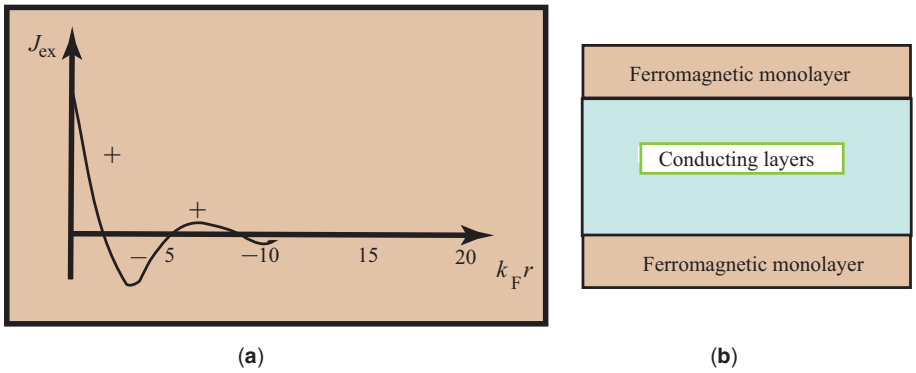

Figure 23. (**a**) Spatial dependence of the RKKY exchange interaction and (**b**) magnetic bilayer system with intervening conducting layer that exhibits an RKKY exchange interaction.

In describing RKKY interactions we consider a polarization plane wave emanating from a magnetic ion at a position $r = 0$. The first waves influenced by a polarizing field are those with wavevector $k = k_F$ and therefore the sign of the exchange interaction oscillates spatially like $\cos(\vec{k}_F \cdot \vec{r})$ as well as decaying exponentially as a function of r. To determine the sign of the indirect exchange interaction between the magnetic ion at $r = 0$ and at $r = r$ we calculate $\cos(\vec{k}_F \cdot \vec{r})$. The RKKY exchange is weaker in magnitude and oscillates in sign spatially and can be described as

$$J_{RKKY} = J_0(r)\cos(\vec{k}_F \cdot \vec{r}) \tag{55}$$

where the prefactor $J_0(r)$ decays exponentially with r.

RKKY interactions are important in a variety of thin film magnetic multilayer devices such as *spin valves*. These have interactions between 2D ferromagnetic layers that are coupled through a conducting layer (Fig. 23b). By varying the thickness of the conducting layer, the sign and magnitude of the exchange interaction can be varied.

Random Exchange

Because of large deviations in interatomic spacings in amorphous alloys as compared with bulk crystalline, they have distributed exchange interactions that alter the mean field description of the temperature dependence of the magnetization, $M(T)$ (Chien, 1978; Kaneyoshi, 1984). A mean field theory for the T dependence of the magnetization in amorphous alloys has been proposed by Kobe (1969) and Handrich (1969). In this *Handrich–Kobe theory* was proposed an expression for the reduced magnetization $m(T) = \frac{M(T)}{M(0K)}$ that consisted of a modified Brillouin function where a single exchange parameter was replaced by an exchange parameter reflecting the distribution of nearest neighbor positions in the amorphous phase. This is expressed as follows:

$$m(T) = \frac{1}{2}\left(B_s[(1+\delta)x] + B_s[(1-\delta)x]\right) \tag{56a}$$

where

$$x = \frac{3S}{S+1}\frac{m}{T}, \qquad t = \frac{T}{T_c}, \qquad \delta = \sqrt{\frac{\langle \Delta J_{ex}^2 \rangle}{\langle J_{ex} \rangle^2}} \tag{56b}$$

The first expression is the argument of a conventional (spin-only) Brillouin function. The *exchange fluctuation parameter*, δ, is defined by the second expression. This parameterizes the root mean square (rms) fluctuation in the exchange interaction. The root mean square exchange fluctuation has been suggested to have a T dependence of the form (Bhatnagar, 1984) $\delta = \delta_0(1-t^2)$. Figure 24a compares mean field results for $M(T)$ in the classical, spin-only, and total angular momentum representations. Figure 24b shows mean field results for $M(T)$ taking into account the disorder-induced fluctuations in the exchange parameter in hypothetical amorphous

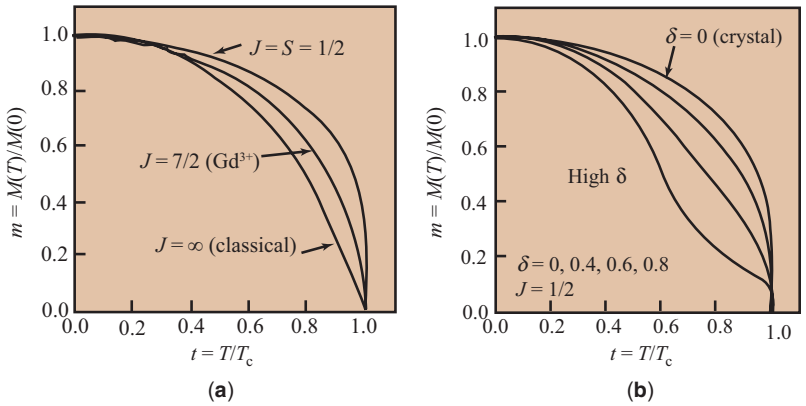

Figure 24. Comparison of magnetization as a function of reduced temperature t (**a**) in a spin-only ferromagnet (using a $J = \frac{1}{2}$ Brillouin function), for $J = \frac{1}{2}$ and for the classical limit $J = \infty$, and (**b**) in an amorphous magnet with $J = \frac{1}{2}$ and different values of the exchange fluctuation parameter δ (figure courtesy of Hiro Iwanabe).

alloys. This construction then predicts a quite remarkable change in the mean field theory thermomagnetic response for amorphous magnets.

The T dependence of the magnetization for $Fe_{88}Zr_7B_4Cu$ amorphous alloy has been measured by Gallagher et al. (1999). A two-parameter exchange fluctuation mean field theory is shown to give significantly better fits than the single-parameter Handrich–Kobe model to $m(T)$ for these amorphous alloys. The deviation in atomic nearest neighbor (NN) distances in this amorphous alloy was estimated from X-ray scattering data. The Bethe–Slater curve was used to estimate fluctuations in the exchange interaction. An explanation for the relative invariance of $M(T)$ in disordered Co-based alloys as compared with Fe-based alloys was proposed and good qualitative agreement of the model and experimental data has been demonstrated. The modification made to the Handrich–Kobe (Kobe, 1969; Handrich, 1969) equation allowed for two δ parameters, δ_+ and δ_- (Fig. 25). The new equation is as follows:

$$m(T) = \frac{1}{2}(B_s[(1+\delta_+)x] + B_s[(1-\delta_-)x]) \qquad (57)$$

where δ_+ and δ_- are not necessarily the same and therefore can act as a first-order fit to an asymmetric distribution function. The *Gallagher* (Gallagher et al.,1999) model gives a better quantitative fit to the temperature dependence of the magnetization.

MICROSCOPIC MAGNETIZATION AND DOMAINS

A *magnetic domain* is macroscopic volumes over which atomic magnetic moments are aligned. For a ferromagnet, when $H_a = 0$, the existence of a spontaneous magnetization requires the existence of domains. It is perhaps surprising that ferromagnetic materials can exist in a "virgin state" for which the magnetization is zero in the absence of an applied field. This is understood by ferromagnetic domain theory. In a typical magnetic

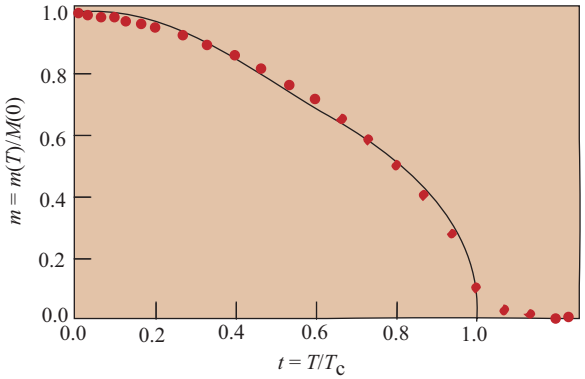

Figure 25. Reduced magnetization, m, as a function of reduced temperature, t, in an amorphous $Fe_{88}Zr_7B_4$ alloy fit with two asymmetric exchange fluctuation parameters, δ_+ and δ_- (Gallagher et al., 1999).

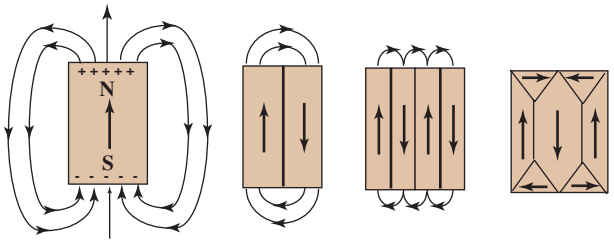

Figure 26. Reduction in the demagnetization field as a result of the introduction of magnetic domains into a ferromagnetic sample.

material a macroscopic volume contains many domains. Each domain has a spontaneous magnetization of magnitude, M_s. In the absence of an applied field the magnetization vectors are randomly aligned from domain to domain (just like in a paramagnet atomic dipoles were random). Taking a vector sum of the magnetization over many domains yields zero sample magnetization because of vector cancellation.

We can qualitatively understand this by recognizing that magnetic flux line leaves the north pole of a magnet and enters the south pole. This gives rise to a field outside the magnet, the *demagnetization field*, H_d, which would like to misalign the dipole moments in the ferromagnet. It requires internal energy to maintain the alignment of the dipoles.

A configuration for which the demagnetization field is reduced will lower the total energy of the system. For two domains (Fig. 26) we significantly reduce the return path that is necessary to be taken by fringing fields. By applying successively more domains we can further reduce the *magnetostatic self-energy* to nearly zero. In the case where we have two long domains and two closure domains the magnetization makes a nearly circuitous path reducing the demagnetization field to nearly zero. There is no free lunch, though. Each boundary between domains requires that we pay an energy associated with a *domain wall*. The configuration of domains and walls ultimately depends on the balancing of these two energies.

CONCLUSIONS

The basic notions of magnetic dipole moments and magnetization in solids have been summarized. In particular, the origin of magnetic dipoles from an atomic, a band structure, and a shielding current (superconductors) picture has been described. The coupling of magnetic dipoles, the field and temperature dependence of the magnetization, and simple magnetic phase transitions have been illustrated. This serves to define certain basic magnetic phenomena that will be elaborated on, illustrated, and extended in subsequent units. Magnetic phenomena are rich and varied; the fundamental principles of the origin, coupling, and vector summation of magnetic dipole moments are at the heart of a comprehensive understanding of magnetic phenomena.

BIBLIOGRAPHY

LITERATURE CITED

Abrikosov, A. A. 1957. On the magnetic properties of superconductors of the second group. *Sov. Phys. JETP-USSR* 5 (6):1174–1183.

Bhatnagar, K., Prasad, B. B. and Jagannathan, R. 1984. *Phys. Rev. B*, 29. 4896.

Bethe, H. A. and Sommerfeld, A. 1933. Handbuch der Physik, Vol. 24. Springer, Berlin.

Chien, C. L, 1978. Mossbauer study of a binary amorphous ferromagnet: Fe_{80} B_{20}, *Phys. Rev. B.* 18:1003–15.

Cullity, B. D. and Graham, C. D. 2009. Introduction to Magnetic Materials, 2nd ed. IEEE Press/John Wiley and Sons, Hoboken, NJ.

de Gennes, P. G. 1966. Superconductivity of Metals and Alloys. Benjamin, New York.

Diaz-Michelena, M. 2009. Small magnetic sensors for space applications. *Sensors* 9:2271–2288.

Diggs, B., Zhou, A., Silva, C., Kirkpattrick, S., McHenry, M. E., Petasis, D., Majetich, S. A., Brunett, B., Artmen, J. O., and Staley, S. W. 1994. Magnetic properties of carbon-coated rare earth carbide nanocrystals produced by a carbon arc method. *J. Appl. Phys.* 75:5879.

Fisher, M. P. A. 1989. Vortex-glass superconductivity: A possible new phase in bulk high-Tc oxides. *Phys. Rev. Lett.* 62:1415.

Friedel, J. 1958. Theory of magnetism in transition metals. *Nuevo Cim. Suppl.* 7:287.

Gallagher, K. A., Willard, M. A., Laughlin, D. E., and McHenry, M. E. 1999. Distributed magnetic exchange interactions and mean field theory description of temperature dependent magnetization in amorphous $Fe_{88}Zr_7B_4Cu_1$ alloys. *J. Appl. Phys.* 85:5130–5132.

Ginzburg, V. L. and Landau, L. D. 1950. *Zh. Eksp. Teor. Fiz.* 20:1044.

Handrich, K. 1969. A Simple Model for Amorphous and Liquid Ferromagnets. *Phys. Status Solidi.* 32:K55.

Harrison, W. A. 1989. Electronic Structure and the Properties of Solids: The Physics of the Chemical Bond. Dover Publications, New York.

Heisenberg, W. 1928. On the theory of ferromagnetism. *Z. Phys.* 49:619.

Hund, F. 1927. Linienspektren und periodische system der elemente. Springer, Berlin.

Kammerlingh-Onnes, H. and Tuyn, W. 1929. *Leiden Comm.* 198.

Kaneyoshi, T. 1984. Amorphous Magnetism Chemical Rubber Corp., Boca Raton, FL.

Kasuya, T. 1956. Electrical resistance of ferromagnetic metals. *Prog. Theor. Phys.* 16:45.

Kobe, S. 1969. *Phys. Status Solidi.* 32:K55.

Kobe, S. 1970. ibid. 41:K13.

Kobe, S., Handrich, K., Tverd, Fiz. and Leningrad, Tela. 1971. 13, 887 and *Sov. Phys. Solid State.* 13:734.

Langevin, P. 1907. Magnetisme et Theorie des Electrons. *Ann. Chem. Phys.* 5:70.

London, F. 1950. Superfluids, Vol. 1. John Wiley and Sons, New York.

MacLaren, J. M., McHenry, M. E., Eberhart, M. E., and Crampin, S. 1990. Magnetic and electronic properties of Fe/Au multilayers and interfaces. *J. Appl. Phys.* 61:5406.

MacLaren, J. M., Schulthess, T. C., Butler, W. H., Sutton, R. A., and McHenry, M. E. 1999. Calculated Exchange Interactions and Curie Temperature of Equiatomic B2 FeCo. *J. Appl. Phys.* 85:4833–35.

Maley, M. P., Willis, J. O., Lessure, H., and McHenry, M. E. 1990. Dependence of flux creep activation energy upon current density in grain-aligned YBa2Cu3O7-x. *Phys. Rev. B* 42:2369.

McHenry, M. E. and MacLaren, J. M. 1991. Iron and chromium monolayer magnetism in noble-metal hosts: Systematics of local moment variation with structure. *Phys. Rev. B* 43:10611.

McHenry, M. E., MacLaren, J. M., Eberhart, M. E., and Crampin, S. 1990. Electronic and magnetic properties of Fe/Au multilayers and interfaces. *J. Magn. Magn. Met.* 88:134.

McHenry, M. E. and Sutton, R. A. 1994. Flux pinning and dissipation in high temperature oxide superconductors. *Prog. Met. Sci.* 38:159.

Meissner, W. and Ochsenfeld, R. 1933. Ein neuer Effekt bei Eintritt der Supraleitfahigkeit. *Naturwissenschaften* 21:787–788.

Neel, L. 1932. Influences des Fluctuations du Champ Moleculaire sur les Proprietes Magnetiques des Corps. *Ann. Phys.* 18:5–105.

Nelson, D. R. 1988. *Phys. Rev. Lett.* 60:1973.

Onnes, H. K. 1911. The superconductivity of mercury. *Commun. Phys. Lab. Univ. Leiden* 122, 124.

Onnes, H. K. and Clay, J. 1908. On the change of the resistance of the metals at very low temperatures and the influence on it by small amounts of admixtures. *Commun. Phys. Lab. Univ. Leiden* 99c:17–26.

O'Handley, R. C. 1987. Physics of ferromagnetic amorphous alloys. *J. Appl. Phys.* 62 (10):R15–R49.

O'Handley, R. C. 2000. Modern Magnetic Materials, Principles and Applications. John-Wiley and Sons, New York.

Pauling, L. 1938. The nature of the interatomic forces in metals. *Phys. Rev.* 54:899.

Ruderman, M. A. and Kittel, C. 1954. Indirect exchange coupling of nuclear magnetic moments by conduction electrons. *Phys. Rev.* 96:99.

Russell, H. N. and Saunders, F. A. 1925. New regularities in the spectra of the alkaline earths. *Astrophys. J.* 61:38.

Slater, J. C. 1930. Atomic shielding constants. *Phys. Rev.* 36:57–64.

Slater, J. C. 1937. Electronic structure of alloys. *J. Appl. Phys.* 8:385.

Van Vleck, J. H. 1932. The Theory of Electric and Magnetic Susceptibilities. Oxford University Press, New York.

Weiss, P. 1907. L'hypothese du Champ Moleculaire et la Propriete Ferromagnetique. *J. Phys.* 6:661.

Yafet, Y. and Kittel, C. 1952. Antiferromagnetic arrangements in ferrites. *Phys. Rev.* 87 (2):290–294.

Yosida, K. 1957. Magnetic properties of Cu–Mn alloys. *Phys. Rev.* 106:893.

KEY REFERENCES

Solid State Physics Texts—Introductory (Undergraduate) Level

Eisberg, R. and Resnick, R. 1974. Quantum Physics of Atoms, Molecules, Solids, Nuclei and Particles. John Wiley and Sons, New York.

Rosenberg, H. M. 1990. The Solid State. Oxford Science Publications, Oxford.

Solymar, L. and Walsh, D. 1998. Lectures on the Electrical Properties of Materials. Oxford University Press, New York.

Solid State Physics Texts—Intermediate to Graduate Level

Ashcroft, N. W. and Mermin, N. D. 1976. Solid State Physics. Holt, Rinehart and Winston, New York.

Blakemore, J. S. 1981. Solid State Physics. Cambridge University Press, Cambridge, UK.

Burns, G. 1985. Solid State Physics. Academic Press, San Diego, CA.

Kittel, C. 1976. Introduction to Solid State Physics. John Wiley and Sons, New York.

Physics of Magnetism

Chikazumi, S. 1978. Physics of Magnetism. Kreiger, Malabar, FL.

Keefer, F. 1982. Helimagnetism. In McGraw-Hill Encyclopedia of Physics (S. P. Parker, ed.). McGraw-Hill, New York.

Morrish, A. H. 1965. The Physical Principles of Magnetism. Wiley, New York.

Mydosh, J. A. 1993. Spin Glasses, An Experimental Introduction. Taylor and Francis, London, Washington, DC.

White, R. M. 1983. Quantum Theory of Magnetism, Springer Series in Solid State Physics 32. Springer-Verlag, Berlin.

Magnetic Materials

Berkowitz, A. E. and Kneller, E. 1969. Magnetism and Metallurgy, Vol. 1. Academic Press, San Diego, CA.

Bozorth, R. M. 1951. Ferromagnetism. Van Nostrand, New York.

Chen, C.-W. 1986. Metallurgy of Soft Magnetic Materials. Dover, New York.

Coey, J. M. D. 2010. Magnetism and Magnetic Materials, Cambridge University Press, Cambridge.

Cullity, B. D. 2009. Introduction to Magnetic Materials, 2nd ed. IEEE Press, Hoboken, NJ.

Kouwel, J. S. 1969. Magnetism and Metallurgy 2 (A. E. Berkowitz and E. Kneller, eds.), p. 523. Academic Press, New York.

McCurrie, R. A. 1994. Ferromagnetic Materials: Structure and Properties. Academic Press, London.

Morrish, A. H. 2001. The Physical Principles of Magnetism. IEEE Press, New York.

O'Handley, 2000. See above.

Fine Particle and Nanomagnetism

Bean, C. P. and Livingston, J. D. 1959. J. Appl. Phys. 30:120S–129S.

Bitter, F. 1932. Phys. Rev. 38:1903; ibid. 41:507 (1932).

Jacobs, I. S. and Bean, C. P. 1963. Magnetism, Vol. 3 (G. T. Rado and H. Suhl, eds.). Academic Press, New York.

Luborsky, F. E. 1962. J. Appl. Phys. 32:171S–183S.